Title

Articulating the phase-separated microstructure of stearyl acrylate-based thermochromic polymers for application in smart windows

Author

He, Mingfei

Publication Date

2021

Peer reviewed|Thesis/dissertation

UNIVERSITY OF CALIFORNIA

Los Angeles

Articulating the phase-separated microstructure of stearyl acrylate-based thermochromic polymers for application in smart windows

A thesis submitted in partial satisfaction

of the requirements for the degree Master of Science

in Material Science and Engineering

by

Mingfei He

2021

ABSTRACT OF THE THESIS

Articulating the phase-separated microstructure of stearyl acrylate-based thermochromic polymers for application in smart windows

by

Mingfei He

Master of Science in Materials Science and Engineering

University of California, Los Angeles, 2021

Professor Qibing Pei, Chair

Smart windows that are based on thermoresponsive materials are becoming a strong competitive candidate in smart window research since they can dynamically respond to the environmental temperature, granting us comfort and privacy without increasing building energy expenditure. The focus of this study is a thermochromic phase-changing polymer material that can switch between an opaque crystalline phase and a transparent amorphous phase. The two major constituents of the polymer film are stearyl acrylate and ethoxylated trimethylolpropane triacrylate, both acrylate compounds. At room temperature, the polymer film possesses a semi-crystalline structure that scatters visible light and infrared efficiently. Above the transition

temperature, the film undergoes order-to-disorder structural transition thus becomes light-transmitting. The fabricated film in this study presented 71.4% transmission modulation over the whole solar spectrum, 70.9% for the visible light modulation, and 68.5% for the infrared modulation.

The thermoresponsive polymer layer in this study is equipped with a polyurethane acrylate-based, transparent heater embedded with silver nanowires that heats the polymer film through joule heating until it reaches the transition temperature. The fabricated composite transparent heater is also capable of achieving fast heating speed while maintaining high visible transparency and long-term thermal stability. A smart window device was assembled by sandwiching the thermochromic layer (150 μm) between the transparent heater layer (90 μm) and pure polyurethane acrylate protection layer (90 μm). By switching on and off the DC power source, the device can switch freely between opaque and transparent states according to personal needs.

The thesis of Mingfei He is approved.

Bruce S. Dunn

Ximing He

Qibing Pei, Chair

University of California, Los Angeles

2021

TABLE OF CONTENTS

LIST OF FIGURES

ACKNOWLEDGMENT

I would like to express my gratitude here to everyone who supported me during my graduate study, especially during these special times last year. I would like to first thank my research supervisor, Prof. Qibing Pei, for providing me with this opportunity to be a part of this group and participating in the study of smart window films. I would like to thank Dr. Yu Xie and Fangyi Guan, who have been previous members of the lab, for their guidance at the early stage of my thesis work. I would also express my appreciation to other lab members, especially to Ying Liu, for the advice and collaboration in improving the fabrication process; and Jiacheng Fan, for the collaboration in film characterization. Lastly, I am grateful for having a supportive family that provided me the platform to study abroad and supported me during my time at UCLA.

Chapter 1 Introduction

1.1 Current situation of Energy consumption

The rapid increase in energy consumption in current society has become a concerning topic in modern days due to the worsening of our environment and the exhaustion of traditional energy sources. Among all the sectors, buildings consume an extensive amount of energy, in developed countries, it could contribute up to 40% of total energy usage. Heating, ventilation, and air conditioning (HVAC) systems in buildings are the largest energy end-use both in the residential and non-residential sector and are increasing in the past few decades [1,2] Therefore, reducing the energy cost of buildings is essential to the reduction of the total energy cost of the society.

The windows installed in buildings serve not only as the passage of light during daytime but also as a medium of heat transfer. Windows are often considered to be energy-inefficient due to the large heat transfer coefficients that allow heat to dissipate through glazing, usually in a direction that is contrary to what is desired. [3,4] To reduce the energy consumption of windows, it is necessary to develop and adopt new novel features and functions on the basis of traditional glass windows to improve their thermal properties.

Recently, researchers have been making progress on the development of a new type of window, smart windows. Dynamic and reversible thermoregulation can be achieved by applying smart window technology, and there have been many developments in the last decade. The transformation of smart windows between different states can be triggered by external stimuli or personal preference, to actively and reversibly regulate the solar radiation that enters the room. These windows not only ensure indoor lighting but also reduce reliance on artificial lighting and

air conditioning, thus reducing energy loss and minimizing energy usage. [5] Previous studies have shown that smart window technology can save up to 40% of energy compared to the conventional static glass windows in a building. Light management using advanced smart window technologies can theoretically lead to annual energy savings of more than 1.055×10^{15} kJ in the United States, which is equivalent to 1% of annual total energy consumption. [6-8] Hence study regarding the smart window technology is necessary and undoubtedly beneficial to us humans as a society in the future.

1.2 Overview for smart windows

1.2.1 Mechanism of smart windows

The concept of smart window technology involves many aspects, from anti-scratch, self-healing to dynamic daylight control. The daylight control in smart window technology can provide both indoor thermal and visual comfort while improving building energy efficiency. Ideal smart windows should be able to regulate two types of radiation, solar radiation and long-wavelength thermal radiation emitted by indoor objects. The window will allow solar radiation to transmit through during summer to reduce heat load so that a comfortable indoor environment can be maintained, while in winter gain full energy harvesting from solar radiation. At other times, the user can achieve direct control in relation to external daily environmental conditions and personal needs. [9] In the meanwhile, the window can possess high visual transparency to properly function as a window.

The schematics of the working mechanisms of a conventional glass window and a perfect smart window are displayed in Figure 1-1. A conventional window does not regulate solar radiation, therefore solar radiation and thermal radiation transmission do not meet many

obstacles. An excess of IR enters the room in summer and too much thermal radiation leaves the room in winter. As a comparison, ideal smart windows are able to regulate both solar radiation and thermal radiation. During hot seasons, the windows hinder IR entering but allow visible light to transmit through to contribute to indoor lighting; thermal radiation is free to escape from the room. While in cold seasons, solar radiation transmission is permitted, and thermal radiation is blocked. To achieve that, the window needs to experience a state change that can be activated through various elements. Therefore, the currently available smart window materials can be divided into four main categories, photochromic, electrochromic, mechanochromic and thermochromic. Among them, photochromic and thermochromic make passive devices while electrochromics and mechanical devices are active devices. [10-16]

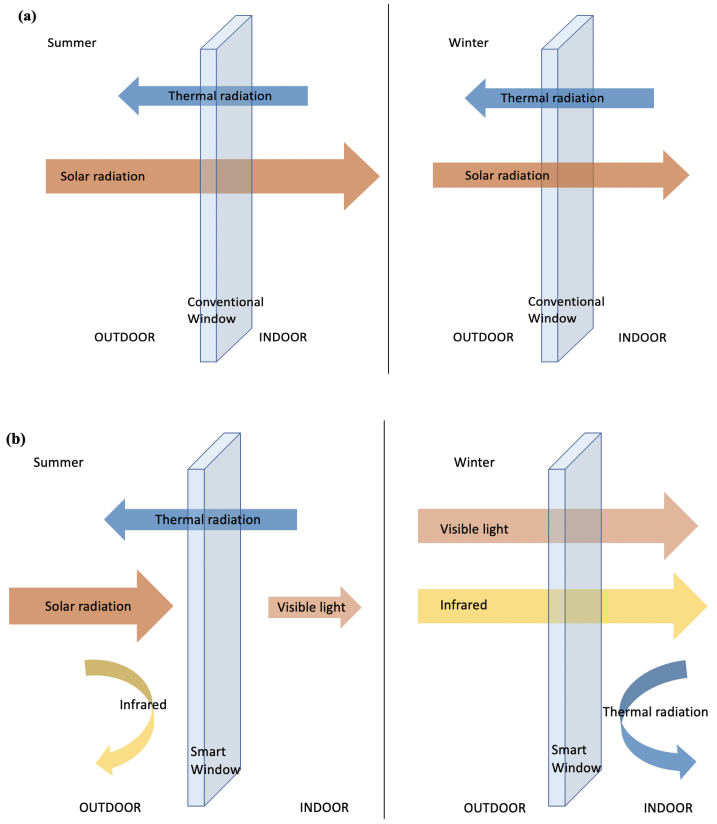

Figure 1-1. The illustration of behavior of a conventional window (a) and an ideal smart window (b) during summer and winter.

1.2.2 Photochromic materials

Photochromic materials, such as tungsten oxide (WO_3) or antimony−tin oxide (ATO) with their composites, utilize UV radiation to induce a change in oxidation state, resulting in a change in color that can regulate the amount of incoming sunlight. Photochromic smart windows have the advantage of self-adaptive transmission as long as solar radiation exists. However, the response time for a photochromic smart window can take up to 15~40 minutes, and additional artificial lighting is necessary since there is no guarantee that enough sunlight can transmit through. Moreover, photochromic materials usually have an absorption peak in the visible light region, resulting in fixed coloration, which is not a desired feature for applications like windows. [17-22]

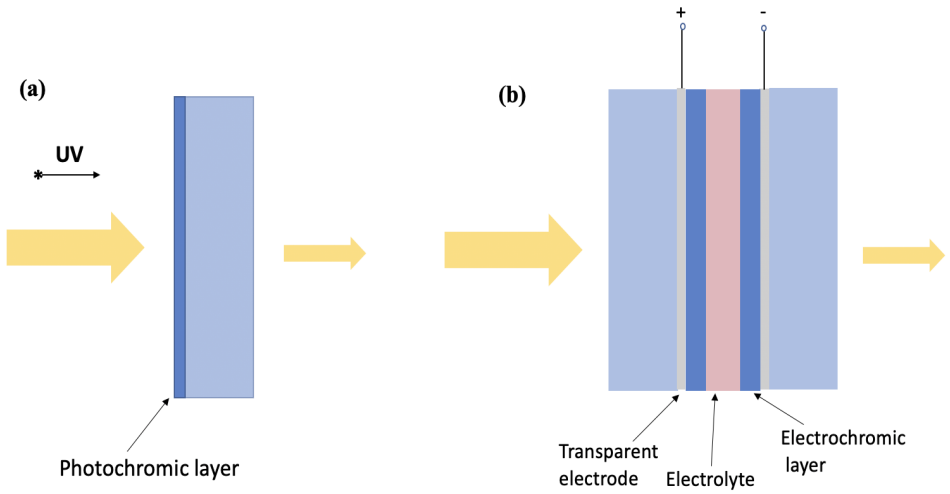

Figure 1-2. Mechanism of a photochromic smart window (a) and an electrochromic device (b).

1.2.3 Electrochromic materials

Electrochromic materials, including metal oxides and polymers, have become a popular option for smart windows since this type of material enables dynamic and independent control of the optical property. Electrochromic windows usually adopt a sandwich structure that consists of electrochromic material, transparent electrodes (e.g., indium tin oxide (ITO) glasses), and ion-conducting electrolytes. [15] The switching between different light transmitting modes relies on the reversible oxidation and reduction processes of the electroactive layer. The material undergoes a redox reaction when an applied voltage is applied, enabling the dynamic control of visible light and solar heat passing through building windows. The best well-known electrochromic materials nowadays are metal oxides and electrochromic conducting polymers. [3]

Metal oxide electrochromic devices usually exhibit remarkable electroresponsive properties. WO_3 electrochromic windows were first studied and remain the most promising and most applied candidate among all the materials due to their largest modulation range among all the devices. The simplified reaction is represented by: WO_3 (transparent) + $xM^+ + xe^- \leftrightharpoons M_xWO_3$ (deep blue), where M^+ can be H^+, Li^+, Na^+ or K^+. Other than WO_3, some other metal oxides such as nickel oxide (NiO), iridium oxide (IrO_2 and Ir_2O_3), niobium pentoxide (Nb_2O_5), Bi_2O_3, CoO etc. are used. [3] Zhang et al. selected monoclinic oxygen-deficient tungsten oxide nanowires (m-WO_{3-x} NWs) as the electrochromic host for Al^{3+} intercalation/de-intercalation. [23] Al^{3+} can inject three times as many electrons for the same number of ions compared to monovalent ions, such as commonly used corrosive H^+, high-cost Li^+, and large Na^+, thus leading to higher efficiency, cheap and stable devices plus environmental friendliness. By varying the applied

voltage, researchers were able to achieve independent dual-band modulation of NIR and visible light to switch to bright mode, cool mode at a lower potential and dark mode at even lower potential.

Metal and metal oxide–polymer hybrids have become a new prospect in electrochromic devices. Gel-type polymer electrolytes such as polymethyl methacrylate (PMMA), poly(propylene glycol), poly(propylene oxide), etc, offers a stable interface, high ion conductivities, and high transmittance, while conventional solid-state electrolytes are limited by slow switching speed attributed to the lower mobility of the ionic species that reduce transparency. Such electrochromic windows have already been installed on Boeing 787 planes. [15] The hybrid electrochromic devices either involves aligning nanowires, such as TiO_2 or Ag, inside the polymer matrix using the applied electric field in order to alter the optical properties [24], or controlled aggregation of the nanoparticles to scatter light or transmit light according to the attached chain length [25].

Conducting polymer electrochromic materials, such as polypyrrole, polyaniline (PANI), and poly(3,4-ethylene-dioxythiophene) (PEDOT), are also available. PANI has shown long-term electrochemical cycling stability over 10^6 cycles, plus its low cost and easy processing advantages make PANI a welcoming research target. PEDOT has the advantage of easy coloring and fast response times, but the electrochromic contrast is a relatively weak one. [3]

For electrochemical materials, the mechanism of transmission modulation is the reversible insertion of extractions of ions and electrons in the redox reactions. [3] The switching time is determined by ion diffusion length and surface area with the electrolyte, and the cycling ability is limited by the electrolyte. [26] The areas of improvement include adopting new structural designs, [27] doping [28], or compositing with a complementary electrochromic

material to improve electrons diffusion efficiency. [29] The nanostructure is used to shorten ion diffusion length and enlarge surface area with electrolyte to result in faster switching and a longer lifetime. Not only nanowires are used, but also nanorods or nanotubes in 1D and sheets in 2D. [30] Nonetheless, electrochromic windows have problems like fixed coloration and costly electrolytes that still desire further development. [31]

Another category in electrochromic windows is liquid crystal (LC) windows, based on cholesteric liquid crystal materials, which can be aligned with or perpendicular to the direction of the applied electric field to alter light transmittance. [32-34] Chiral dopants in cholesteric-nematic liquid crystals can be used to adjust pitch between successive layers of nematic LC, resulting in a change in the central reflection band. LC smart windows can possess bistable or multistable property under different driving frequencies, thus achieving the goal of an energy-saving and safe driving environment. [35,36] However, the bandwidth of the reflection band is often restricted to 100~200 nm, therefore has limited effects on Near-Infrared (NIR) reflection. Lamination of LCs with different pitches or creating a pitch gradient in a single layer are two possible solutions to this problem, nonetheless, both methods cause an increase in the haze at a transparent state as well as adding to the complexity and cost of device manufacturing. [37]

1.2.4 Mechanical-responsive composite materials

Mechanical actuation of composite materials has become a new approach in thermoregulation due to its advantage in low installation cost and maintenance cost. [15] These materials are generally based on IR and optically transparent stretchable elastomers, such as Polydimethylsiloxane (PDMS) [15] or polyethylene derivatives [38]. Approaches based on periodic nano- and microstructured elastomers, including micro-and nanopillar arrays, [39]

wrinkles [40], and 3D photonic crystals [41]. For dye-containing elastomers that possess micro or nanostructures, they are opaque at the initial state due to light scattering, and the transmittance increases when experiencing mechanical stretching or compressing. As for nanoparticle-containing composites, the inter-particle spacing changes will lead to localized surface plasmon resonance (LSPR) change, reshaping the plasmon absorption peak and the absorption intensity. [15]

Recently, mechanical-responsive composite materials have drawn lots of attention regarding their application for smart window purposes. The device tends to consist of a transparent component and a light-blocking component, and the mechanical force will be used to organize the two parts to allow light transmission or blocking. One approach is using a soft, stretchable IR-transparent polymer matrix, such as polyethylene derivatives, overlaid with an array of IR-reflecting metal/oxide columnar nanostructures [38], alternating laminated oxide layers [42], or silica nanoparticles surrounded by wrinkles and nanovoids [43]. When strain is applied, the surface morphology will experience a reversible change that allows a device equipped with the composite material to reflect or transmit IR. After strain is removed, the original structure is restored. Such a device with dynamic thermoregulation ability has the advantage of a fast response. In another pressure-responsive case, modulation ability is achieved by the reversible formation and breaking of hydrogen bonding between the agar and hydrogel layers, the transition time for such devices can switch as fast as 35 milliseconds, with a 50% transmittance change. [44] However, a relatively large strain (over 10%) is usually needed for switching in strain-induced cases, which is hard to accomplish in building applications, and applying pressure consistently is also impractical for commercial buildings. Lastly, the fatigue life under mechanical loading still needs further development for safety reasons. [10,45]

1.2.5 Thermochromic materials

Thermochromic-based smart windows have drawn a lot of attention in recent years for the advantages of low cost, simple fabrication process, and dynamic response to environmental changes. The passive operation nature and relatively simple structure are highly desirable features of smart window applications. When applied on windows, thermochromic materials can be designed to help improving building energy efficiency while reducing glare and overheat. [46]

Conventional thermochromic windows based on VO_2 that experience a reversible structural phase transition at critical temperature (68°C), from monoclinic at low temperature to high-temperature tetragonal rutile phase, providing huge transmittance contrast at the near-infrared range. However, reducing the critical temperature while maintaining the material's luminous transmission and IR modulation ability has been proved to be a challenging task and still requires further development for practical uses. The high transition temperature either demands the outdoor temperature to be higher than 50°C or a large amount of energy input. [47-49] In some best-performing VO_2 devices in literature the transition temperature can even reach 90°C. The elevated temperature of the surface will undermine the heat shielding ability of the window, with solar transmittance modulation of 22.3% with a luminous transmittance of 45.6% before phase transition. [50] Approaches such as doping and anti-reflective coating have been used on pure VO_2 material for improvement, however, the trade-off between transition temperature and light transmission still prevents VO_2 from applying on products in the market, and the best performing products still have a relatively small modulation range. [50-52] Addition to the performance, the durability of such smart windows remains to be an issue since VO_2 is easy to subject to oxidation. [47,53]

VO_2-based thermoresponsive composites have become promising candidates for smart window applications since a composite can combine the characteristics of thermochromic VO_2 and the polymer matrix to present an enhancement of modulation ability and oxidation resistance [15], such as a VO_2@SiO_2/poly(N-isopropylacrylamide) (PNIPAm) hybrid nanothermochromic microgels reported by Wang et al. [54] A new attempt has been reported by Ke et al. [55] of a VO_2 embedded kirigami structured PDMS as a potential candidate mechano-thermochromic smart window. Adopting the kirigami structure allows the strain to increase to more than 200% and stretching kirigami-structured PDMS creates voids around the nanoparticles that elongate along the stretching direction under increasing strain, leading to dielectric change on the particle surface. When the composite is at a compact state, UV-visible transmittance is restricted but some IR is allowed to transmit through; at stretched state UV-visible is also allowed to pass. The intensity of LSPR gradually increases when the temperature rises due to free electrons released in the phase transition of VO_2 nanoparticles. As a result, absorption in the near-infrared region lowers substantially. The thermal-induced switchable LSPR provides remarkable tunability in the NIR range while the kirigami structure offers the possibility to tune the visible light range. However, limitations such as the additional space required when applying in practice remains.

Thermoresponsive polymer materials can either experience a reversible transparent-to-opaque transition or a transparent-to-colorful transition. The former usually involves a light scattering process and the latter can change the absorption characteristics of a certain visible light band with temperature changes. A bifunctional material can combine the functions of the two types of materials in one, exhibit transparency changes and color change at the same time. [56] In the former situation, thermally induced scattering materials usually consist of two main components and might function according to different mechanisms. For phase separation

systems, the polymers mixed evenly below the switching threshold and phase-separated when the temperature rises, causing light scattering; while for phase-transition systems, the thermotropic additive (domain material) is evenly distributed in the main polymer matrix below transition point and refractive index mismatching leads to light scattering when the temperature is higher. Some other mechanisms include change of the particle size or aggregation of the components. [16] In thermochromic systems, the material experiences thermally driven reversible reactions, caused by charge transfer, bond rearrangements, or stereoisomerism; or structural changes happen in liquid crystals or photonic crystals that result in a shift in absorption peak. [7] For this type of polymer material, coloration is evitable and modulation in the visible light range is limited.

Thermochromic hydrogels have been widely applied in different areas including tissue engineering, drug delivery, and sensors. [57] In the last decade, hydrogel-based thermochromic materials, which utilize the phase separation property of hydrogel to achieve a large modulation range in visible light and near-infrared (NIR) range, have also been a promising candidate for smart window applications. Polymer hydrogel is the aqueous polymer network formed by crosslinking of water-soluble monomers or water-soluble polymers through physical or chemical methods. If the monomer or polymer itself can undergo thermally induced phase separation from water, the hydrogel produced by its crosslinking will obtain thermally induced scattering properties. Below lower critical solution temperature (LCST), the hydrogel is in a swollen state, and hydrogen bondings connect polymers chains and water molecules. When the temperature rises above LCST, bonds are broken and phase separation inside the hydrogel causes a mismatch in refraction index that leads to light scattering. These hydrogel films often suffer from the volume shrinkage or swelling of the entire cross-linked polymer network that results in some

degree of irreversible aggregation during phase transition, so polymer hydrogel has the defect of poor dimensional stability in practical applications. Moreover, since the polymer hydrogel has low mechanical strength, it needs to be encapsulated rigorously in a double-layer glass when used as a heat-induced scattering material for durability. If the packaging process is not performed properly, the thermal scattering characteristics of these materials will gradually decrease with the evaporation of moisture and the destruction of colloids during repeated thermal cycles. [58]

Studies have been focused recently on composite hydrogels for their advantage of multifunctionality or improved performance, such as higher mechanical strength or enhanced solar regulation ability. [57] For instance, PNIPAm based hydrogel composites are the most studied thermoresponsive hydrogels. The polymer matrix that uses benzyl methacrylate-co-octadecyl methacrylate-co-methacrylic acid (BOMA-16) not only exhibits high opacity at room temperature but possesses self-healing property. [59] In another case, the hybrid hydrogel was synthesized with PNIPAm microgel added into a water-rich silica-alumina-based gel matrix, and the resulting material has an effectively enhanced durability. [60] Photo-thermochromic particles such as antimony-doped tin oxide (ATO) gold nanoparticles embedded smart windows utilize absorption-induced heating effect (photothermal effect) to increase color changing speed considerably since well-dispersed ATO can act as nano heaters due to its NIR absorption. [61]

Recent advancements have been achieved in thermally light-diffusing polymers. Compared with hydrogels, polymer blends have a relatively slower thermal response due to the absence of water, but also avoid the issues of encapsulation, mildew, and limited cycle life. [62] Above LCST, components separate above a threshold temperature and the layer becomes light diffusing. In some other cases, the materials change from a light-scattering state to a clear state

as the temperature increases and have been applied for privacy-ensuring purposes, temperature indicators, as well as artistic and information displays. The presence of a second polymer should enhance the light scattering effect at low temperature and serve to maintain the rigidity of the polymers even when the thermal scattering material at high temperatures and guarantee some degree of elasticity at low temperatures. [63]

1.3 Processing of thermochromic materials

The processing of thermochromic materials varies with the type of the material. Traditionally, VO_2 thin films are fabricated through physical vapor deposition, chemical vapor deposition, and the sol-gel process. The sol-gel method is generally considered to be a practical method of thin-film synthesis because of its low cost, easy coating on large-scale surfaces, easy control of reaction kinetics and atomic doping, and reduction of sintering temperature. [64] This method is widely used in the fabrication of metal oxides such as oxides of titanium and silicon. It involves converting the monomer into a colloidal solution, which is used as a precursor to fabricate an integrated network of particles or network polymers. In the case of VO_2 thin film, metallic vanadium powder was first dissolved in a hydrogen peroxide solution to obtain a V_2O_5 precursor. After deposition, the film is annealed at high temperatures, nonetheless, the high annealing temperature leads to difficulty in industrial smart window applications. Nanoscale VO_2 particles can be fabricated through mechanical milling or hydrothermal synthesis. However, these methods also come with a number of intrinsic problems, including low control of nanoparticle performance and expansion of production scale. [65]

1.3.1 Solution-processed polymer thermochromic material

The solution processing method has been applied widely to the fabrication of electronic devices such as solar cells, transistors, thermoelectric devices, sensors, and actuators. [66] Recently, electrochromic smart windows have been fabricated in this way, as well as thermoresponsive ones. Solution-processed polymers have become a novel candidate for smart window applications since this processing method allows lowering manufacturing cost and further fabrication into complex structures. For instance, it has been applied to polymer-assisted deposition of VO_2 films and has shown better control over film thickness, morphology, and optical properties compared to films prepared by gas-phase methods. [67] Solution-processed hybrid micro-nano composite smart material film can easily construct a phase-separated polymer framework containing nanocrystals that achieve fast electro-optical response time, high mechanical strength, and long-term stability. [68]

In this work, the infrared shielding effect of a solution-processed thermochromic phase-changing polymer was studied for smart window (SW) purposes. Stearyl acrylate-based polymers experience a phase change from crystalline to amorphous state when the temperature rises. [69,70] At low temperature, micro-sized aggregated crystalline structure scatters transmitting light, resulting in an opaque stiff film. When temperature increases above the transition point, stearyl acrylate melts into a disordered state, showing a transparent appearance. This ordered-to-disordered change is reversible, making stearyl acrylate-based materials an ideal choice for smart windows.

The characteristics of a smart window can be further improved by involving a copolymer. A second acrylate was added to form a crosslinked polymer network. At low temperatures, the aggregation of polymer networks causes larger crystal size that results in Mie scattering and an

increase in opacity. A solvent is used to co-dissolve the two polymers, in order to improve the miscibility. After curing, phase separation of two distinct polymers leads to an increase in opacity at an opaque state. The uniform distribution of the two components is necessary for a homogeneous smart window film. To ensure this, ultrasonication and heating were applied, as well as a solvent with a low evaporation rate to allow the polymers to form a uniform ordered structure after curing.

To fabricate thermochromic smart windows devices, the combination of thermochromic polymer materials and transparent electric heaters is able to provide passive thermoregulation smart windows with active control and energy-saving effect. Therefore, in this study, the thermochromic interlayer is heated up through Joule heating provided by a silver nanowire embedded transparent layer. The smart window device was tested for visible light and IR-shielding ability and energy saving in the following section.

Chapter 2 Fabrication and Characterization of Phase-Changing Polymer Smart Window Film

The smart window in this work has two major compositions, both are acrylate compounds. Stearyl acrylate is chosen to be the main component due to its transition from a light scattering state at a lower temperature to a light-transmitting state at a higher temperature due to phase change. The other component, Ethoxylated trimethylolpropane triacrylate, is added to enhance film strength and light scattering performance. In this section, the properties and performance of smart window films are examined and compared.

2.1 Experimental

2.1.1 Materials

Stearyl acrylate (SA), 2,2-Dimethoxy-2-phentlacetophenone (DMPA) and trimethylolpropane trimethacrylate (TMPTA) and triton X-100 were supplied by Sigma Aldrich. Ethoxylated trimethylolpropane triacrylate (ETPTA), difunctional acrylic monomer (SR306) and Polyurethane acrylate (CN9009) were supplied by Sartomer.

2.1.2 Fabrication of smart window film

Stearyl acrylate and ETPTA were mixed with a weight ratio of 6:1, 1 wt% of TMPTA was added as the cross-linking agent, 1 wt% of triton X-100 was added to increase the crosslinking of the two acrylates, and 1 wt% of DMPA was added as photo-initiator. The mixture was dissolved in 18~20 wt% Methyl ethyl ketone (MEK) and heated to 80°C until a clear solution was obtained. The smart window precursor was vortexed at about 2000 rpm/min for 2~3

minutes, then sonicated in 100°C water for one minute to give a solution with uniformly mixed components.

The fabrication of a free-standing smart window film is illustrated in Figure 2-1, where the film is pictured as yellow and glass slides as blue. Two glass slides were separated by spacers (170 μm thickness tape) and fixed with tape at short ends. The glass slides and a pipette were then heated on the hot plate at 80°C for 5 minutes to make sure the solution was kept at a high temperature during the entire injection process. The clear, homogeneous solution was then slowly injected using the pipette into space between two glass slides, followed by 3-min UV curing. After cooling down and immersing into the water at room temperature for 10 minutes, the smart window film can be peeled off from the glass slides as a free-standing film with a thickness of roughly 150 μm due to solvent evaporation.

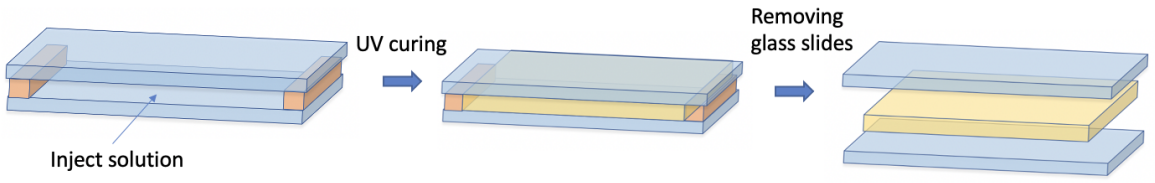

Figure 2.1 The illustration for the fabrication process of smart window film.

2.1.3 Characterization

Scanning Electron Microscope (SEM) images were taken by a Zeiss Supra VP40 SEM using secondary electron mode, accelerating voltage 10.00kV.

A Zeiss microscope was used to observe the film surface from opaque state to transparent state as well as the following cooling recovery process.

Ultraviolet-visible (UV-Vis) spectroscopy is an effective method that studies the structure and composition of material by analyzing the absorption at certain wavelengths, and quantitative analysis can be carried out according to Lambert-Beer law. In this study, the performance of smart window film in terms of visible light/near-infrared shielding effect is evaluated through transmission in 300~2500 nm. The transmittance spectrum displayed for the visible light range (300~800 nm) range was taken using a Shimadzu UV-1700 Pharmaspec spectrophotometer, with a measuring wavelength range of 190~1100 nm. Transmittance spectrum for the visible light and NIR (300~2500 nm) range was taken using a Shimadzu ISR-3100 UV-VIS-NIR spectrophotometer with integrating sphere, equipped with tungsten halogen and deuterium lamps. The measuring wavelength range is 220~2600 nm. During the measurement process, a glass slide was first measured as baseline and auto zeroed, and then transmittance of the sample attached to the glass slide was measured.

X-Ray Diffraction (XRD) uses the scattering effect of electrons on X-rays to obtain information about the crystalline structure, and here it is used to obtain the distribution of the size of crystals in the polymer film. In this study, results were obtained by D8 Advance XRD (Bruker) with Cu Kα radiation, angle repeatability ±0.0001°, absolute accuracy (θ/2θ) ±0.005°.

Differential scanning calorimetry (DSC) is used for thermogravimetric analysis purposes. Here DSC 823e from Mettler Toledo with a heating rate of 10.00 °C min^{-1} was used in order to determine the melting point of the film samples.

Fourier-transform Infrared Spectroscopy (FTIR) is the technique that is used to obtain infrared absorption spectrum. Atoms in chemical bonds selectively absorb infrared light. Therefore, analyzing the absorption spectrum will give enough information regarding the

existence of certain chemical bonds or functional groups. FTIR used in this study is Jasco FT/IR-420 Fourier-transform infrared spectrometer, measuring range 400~4000 wavenumber (cm^{-1}).

2.2 Mechanism of smart window films

Figure 2-2 shows the optical mechanism of the smart window film at opaque and transparent state. Opaque film scatters both visible light and infrared, preventing the transmission through the film. Elevated temperature allows the film to become transparent and therefore acts just like conventional windows. Stearyl moieties experience a reversible order-disorder transition when the temperature changes. Below the transition temperature, the polymer is rigid and light-scattering since the stearyl side chains form crystalline aggregates; at a higher temperature, the aggregates transform to an amorphous structure, so the polymer is soft, flexible, and light-transmitting. [69]

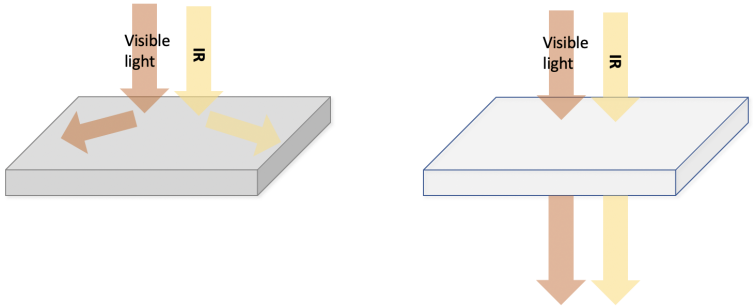

Figure 2-2. Optical mechanism of the smart window film at opaque and transparent state.

2.2.1 Film property characterization

Pure poly (SA) film was fabricated at first, and then the smart window film was prepared from stearyl acrylate and ETPTA. The weight ratio of the two components is selected to be 6:1, since less ETPTA will result in brittle film and too much will interfere with the crystallization

process, leading to a film with low opacity. In the following discussion, characterization graphs for SA and smart window films are presented below in terms of melting point, crystal size, and IR absorption spectrum.

As shown in Figure 2-3, pure SA has a melting point around 32-34 °C, and poly (stearyl acrylate) after curing has a melting point around 48.3 °C, measured by differential scanning calorimetry. As a comparison, a smart window film with two components has a slightly lower melting point, 46.7 °C. The addition of another acrylate lowers the melting point because the growth of polymer molecular chains leads to a lower crosslinking degree. The transition temperature is a crucial factor that could determine the performance of a thermochromic window. The Tm of both samples is in the range that allows them to stay stable at room temperature and do not require much energy input to switch between states. Both SA and smart window film have sharp gradients in the graphs around the melting temperature, indicating the transition from a low-temperature state to a high-temperature state is a sharp endothermic melting process, and this feature is desired by an ideal smart window product.

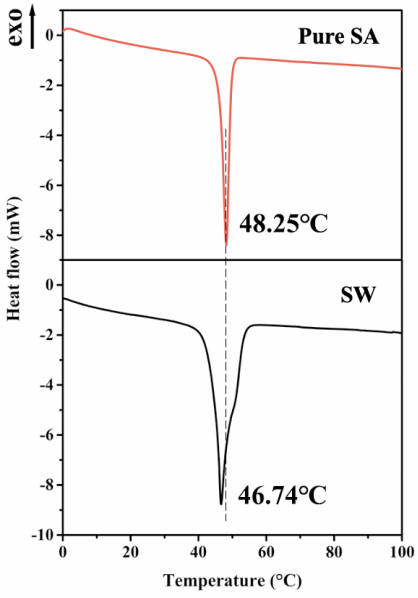

Figure 2-3. Differential scanning calorimetry results of pure poly (SA) and smart window films, showing the melting points.

X-ray diffraction results for SA film and smart window film are presented below as Figure 2-4. The smart window film prepared from two acrylates showed a broader peak and a weaker intensity compared to the SA film, indicating a decrease in crystallite size due to the destruction of the periodic crystal lattice. The size of poly (SA) crystallites can be calculated by the Scherrer equation, which is expressed as: $D = \frac{0.94\times \lambda}{\beta\times cos\theta}$. D is the average crystallite size, β is full width at half maxima (FWHM) in radians, θ is peak position in radians and λ is the X-ray wavelength. The peak position of the SA sample is at 21.5959°, according to the formula, the size of the crystal in poly (SA) is calculated to be around 5.68 nm.

Crystalline poly (SA) film is opaque at room temperature due to light scattering caused by the crystalline region. Rayleigh scattering happens in this case since the crystal size, which is proportional to λ^{-4}, is much smaller than the visible wavelength. Only light with shorter wavelengths can be scattered, and parallel transmittance in the longer wavelength region remains at a high level. The addition of the second component, ETPTA, alters the crystalline structure, resulting in smaller crystal size, thus smart window film presents a wider peak on the XRD spectrum. SA mixing with ETPTA leads to a decrease in ordered SA crystalline regions, the resulting film would create phase separation that is larger than the original crystal size, contributing to Mie scattering, which is relatively wavelength-independent and is the more effective light scattering mechanism for the solar spectrum. Therefore, a smart window film with phase separation between the components can have lower transparency at the opaque state.

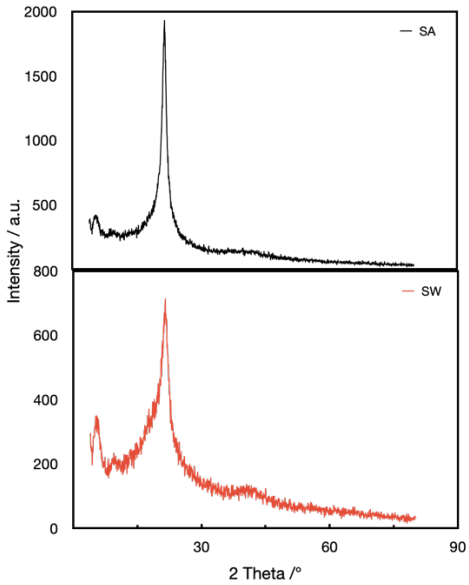

Figure 2-4. X-Ray Diffraction results of pure poly (SA) and smart window films.

FTIR absorption spectrum of pure SA film and smart window film are both displayed in Figure 2-5. C-H stretching in the methylene group has a strong absorption peak that can be found at 2800~3000 cm^{-1} and a medium peak at around 1470 cm^{-1}. In Figure 2-5, poly (SA) has strong peaks at 2960 and 2843 cm^{-1}, and smart window film (SA+ETPTA) has absorption peaks at 2897 and 2836 cm^{-1}. both have a medium peak around 1468 cm^{-1}. C=O stretching in acrylates can lead to a strong absorption peak in 1750-1735 cm^{-1}, and since ETPTA monomer contains three times of C=O bonds than SA monomer, the smart window film presents a much stronger absorption peak at 1743 cm^{-1}. C=C bonds in SA and ETPTA monomers have an absorption peak in 1680-1600 cm^{-1}, but this is not observed in this spectrum, indicating that the double bonds were consumed and polymerization took place.

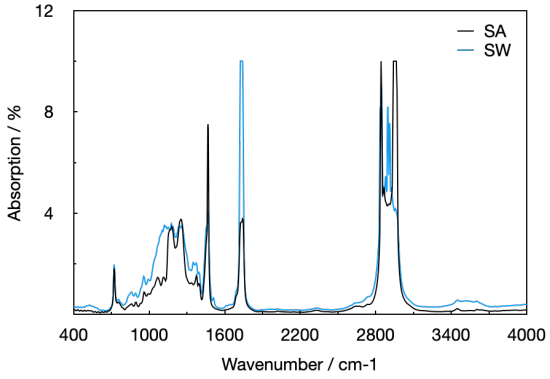

Figure 2-5. FTIR absorption spectrums of Poly (SA) and smart window films.

Differences of surface morphologies between pure poly SA and smart window films at the microscale level are first visualized through SEM images. Images of both films were taken when they were at the opaque state, at ambient temperature. Pure SA has nano-sized particles; hence the film has a smooth surface, and no surface pattern was observed here. On the contrary, the smart window film shows a rough surface with uniformly distributed surface patterns due to the phase separation. The surface of the smart window film clearly presented the micro-sized domains constituted by SA and ETPTA moieties, which contribute to the enhancement of the light scattering effect at longer wavelengths.

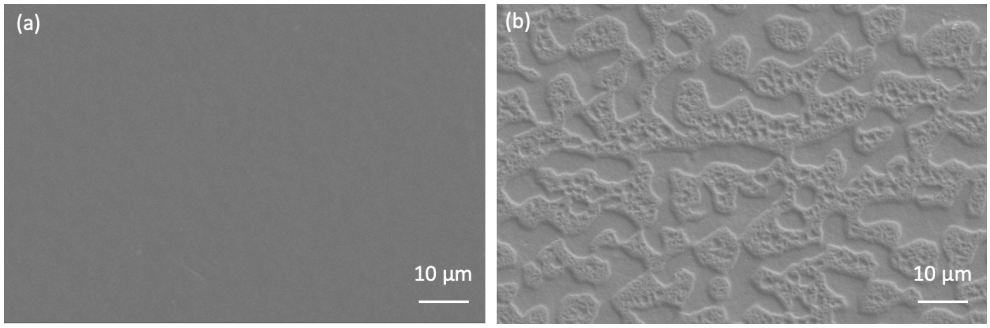

Figure 2-6. Scanning electron microscope images of SA (a) and smart window (b) showing film surface morphology.

Optical images in Figure 2-7 reveal the reversible opaque-to-transparent transition process in situ. At room temperature (25°C), patterns formed due to phase separation can be observed. When the film was then heated to 80°C, the pattern became more flattened and could be hardly observed in the image. This can be explained by the crosslinking bonds still present between two components, however, the shift in crystalline structure resulted in a decrease in phase separation degree, hence is responsible for the increase in transmittance at heated state. The recovering ability is also demonstrated in (c), where the image of the film captured shows that the pattern reappeared after cooling down to 25°C.

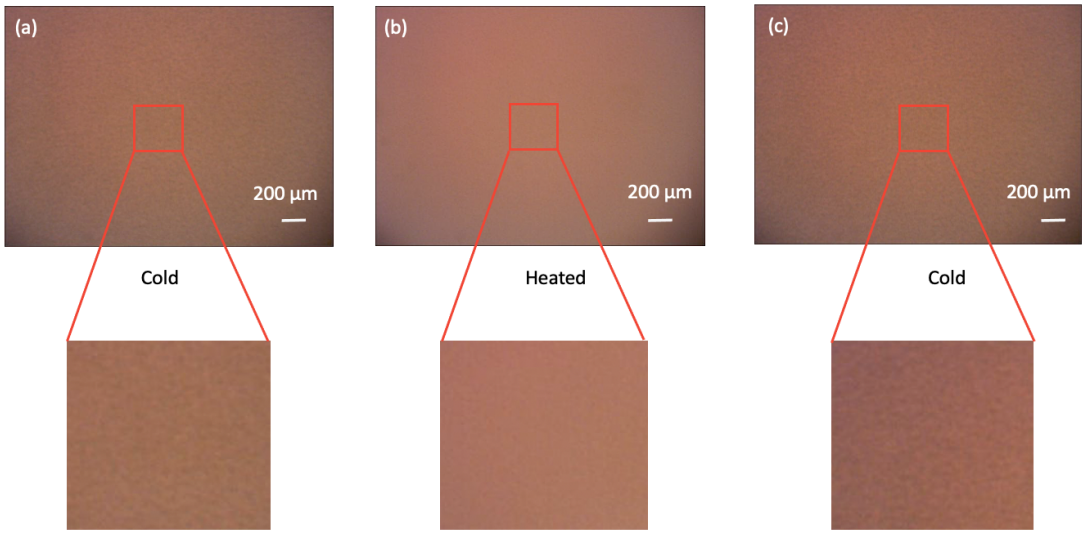

Figure 2-7. Optical images of the smart window film during a transition process. (a) At 25°C, the film at an opaque state displays a clear surface pattern. (b) The film shows a smoothed surface at 80°C. (c) The phase separation pattern reappears when the film returns to room temperature.

2.2.2 Results on light transmittance characterization

UV-VIS-NIR spectrophotometer with integrating sphere attachment was used for full visible light and near-infrared range due to the strong light scattering property of the film samples, and the integrating sphere set can provide more accurate diffusive transmittance measurement results. This is because the measurement lights are irradiated on the light-sensitive surface of the detector after being diffused inside the integrating sphere, while in a conventional detector arrangement scattered light cannot reach the light-sensitive surface of the detector. With both standard plates on, both scattered and scattered light that passes through the sample will be measured. While the film sample's scattered light transmittance is performed with the aperture on so the unscattered light will leave the integration sphere through the open reflection side. The difference between total transmittance and diffusive transmittance is parallel transmittance, the unscattered light.

Schematics for transmittance measurements are shown in Figure 2-8. The thin film sample is placed on a sample holder at the entrance of the sphere. S is for sample beam path and R for reference beam path. Baseline correction is first performed with one glass slide at the aperture of the integrating sphere. Total transmittance is measured with two standard $BaSO_4$ plates attached to the integrating sphere, and diffusive transmittance (scattered light) is measured by removing the plate directly facing the source light. The setup for absorbance measurement is the same as total transmittance, only to set the measured item to absorbance. The measured results are shown in Figure 2-8.

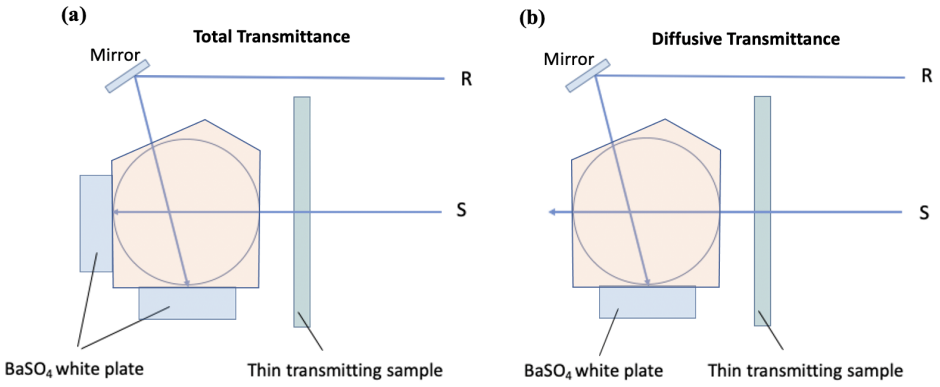

Figure 2-8. Measurement for total transmittance (a) and diffusive transmittance (b), using UV-VIS-NIR spectrophotometer with integrating sphere.

The absorbance in the visible and NIR region at room temperature was measured and found to be less than 1% over the whole range. In the case of thermochromic materials, heat absorbed by the film will lead to unwanted heat entering the room through convection and radiation. High absorptivity at opaque is an undesirable property for the smart window film; therefore, the close to zero solar absorption is beneficial in terms of energy saving. The parallel and diffusive transmittance spectrum of smart window films are presented in Figure 2-9 (b) for the whole solar range (300~2500 nm). At room temperature, the opaque film has low parallel transmittance (7.6% at 550 nm, 25.4% at 1500 nm) and high diffusive transmittance (70.1% at 550 nm, 54.3% at 1500 nm), illustrating that the majority of the incoming visible light and more than half of the IR were scattered by the film. Low visible light parallel transmittance provides privacy for the user, while the slightly higher NIR parallel transmittance still grants the film high modulation capability in terms of energy management. At heated transparent state, the film has high parallel transmittance (80.2% at 550 nm, 79.3% at 1500 nm) and corresponding low diffusive transmittance (7.3% at 550 nm, 2.7% at 1500 nm), indicating the majority of the

incoming visible light and IR transmitted through without scattering, therefore it would behave like a traditional glass window and give good visual and NIR transparency.

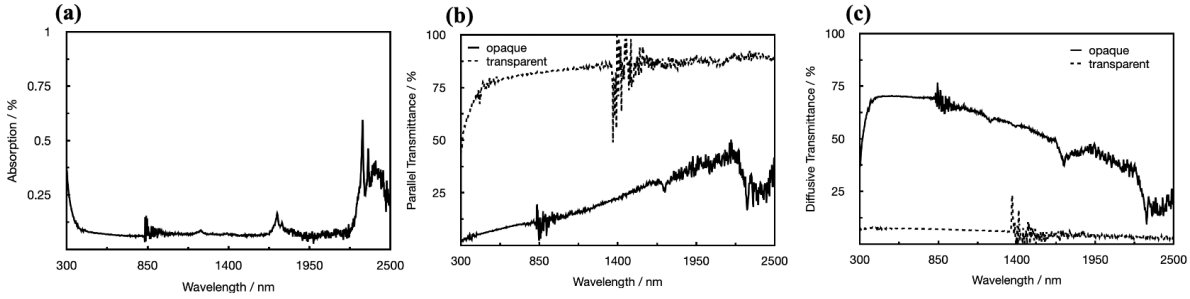

Figure 2-9. Absorption and transmittance spectra of the smart window film. (a) Absorption spectrum in the visible-NIR region. (b) Parallel transmittance spectrum and (c) diffusive transmittance spectrum in the whole solar region.

The modulation ability is evaluated by calculating the difference in transmittance between opaque and transparent states (ΔT). The capability of solar light modulation is assessed through integration of the transmittance over solar, visible and infrared regions. The transmittance is calculated with the following equation:

$$T_{lum/IR/solar} = \frac{\int \varphi(\lambda)\, T(\lambda) d\lambda}{\int \varphi(\lambda)\, d\lambda}) \quad [71]$$

where φ(λ) is the solar radiance spectrum for air mass 1.5 (an inclined plane at 37° tilt toward the equator) in the calculation of T_{solar} and T_{IR}; and φ(λ) is the CIE "physiologically-relevant" luminous efficiency functions for the photopic vision of human eyes in calculating T_{lum}. Solar range here refers to 300~2500 nm, IR range is 780~2500 nm while luminous range is 390~780 nm. T(λ) is the measured transmittance at each specific wavelength. The transmittance modulation ΔT is calculated by subtracting transmittance at opaque from transmittance at transparent state.

The modulation ability in visible and near-infrared regions are demonstrated in Figure 2-10 (a). Opaque transmittance is denoted as the gray columns, transmittance modulation is denoted as the blue columns, so transparent transmittance is the total height of the columns. The overall solar spectrum modulation is 71.4%, where transmittance in the visible region and IR region is 70.9% and 68.5%, respectively. The high ΔT_{lum} indicates effective light scattering in the luminous region, implying the film's potential in user privacy protection, where high ΔT_{IR} indicates that the modulation capability is not confined to the visible spectrum. Since IR is the main contributor to solar energy, the large difference in IR transmittance between two states of the film demonstrates broad bandwidth modulation ability, therefore smart windows based on the film can efficiently control undesired energy transfer in summer and winter, thus contributing to the purpose of total building energy-saving.

The solar modulation ability and visible light transparency of the smart window film is compared with some other thermochromic materials reported in recent years in (b). Transmittance modulation of VO_2 based thermochromic materials (blue squares), hydrogels (green triangles), and smart window film in this work (red dot) are plotted in one diagram with T_{lum} as the x-axis and ΔT_{solar} as the y-axis. Some VO_2 based materials have high luminous transmittance, but the overall modulation ability over solar range is limited. [48-52, 72-73] Hydrogel-based materials generally have high transparency in visible range, and also possess large modulation range for solar regions, sometimes as close to 80%. [58, 74-75] The smart window in this study has great behavior in terms of visual transparency, as well as solar modulation.

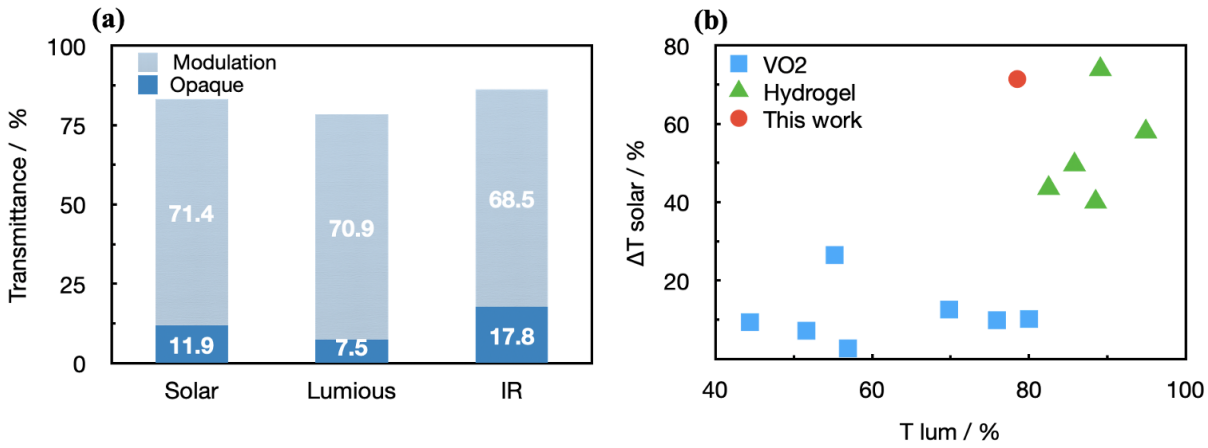

Figure 2-10 (a) Smart window film transmittance modulation for the solar, luminous, and infrared region. (b) Luminous transmittance and solar modulation performance comparison for some thermochromic smart windows, including VO_2 based materials and hydrogel-based materials. [48-52, 58, 72-75]

2.2.3 Reversibility test and demonstration of transition process

The cycling capability, being an important factor in smart window performance evaluation, is assessed through transmittance at 550 nm for 50 cycles with UV-Vis spectrometer, and the parallel and diffusive transmittance of the first and last five cycles are displayed in Figure 2-11. The parallel transmittance changed from around 24% to 87% in one cycle, while the diffusive transmittance changed from 67% to 8%, corresponding to 63% and 59% modulation range, respectively.

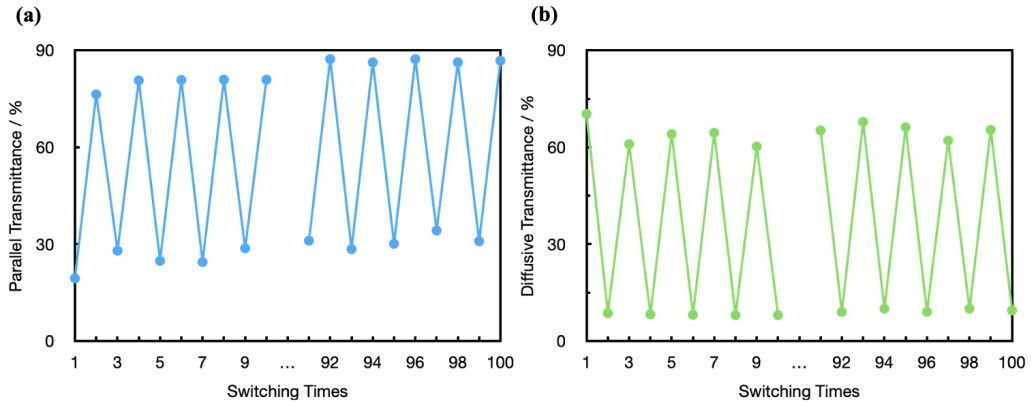

Figure 2-11. Cycling test for the smart window prepared with MEK for 50 cycles. Parallel (a) and diffusive (b) transmittance measured at 550 nm by Shimadzu ISR-3100 UV-VIS-NIR spectrophotometer with integrating sphere.

Figure 2-12 (a) to (c) present a full transition cycle of the smart window film in an actual scene. The original opaque film blocked the picture behind it. After heating up the film, the periodic table in the background displayed a clear shape through transparent film. Then when the film was cooled down to room temperature, it returned to opaque state and the table became concealed again.

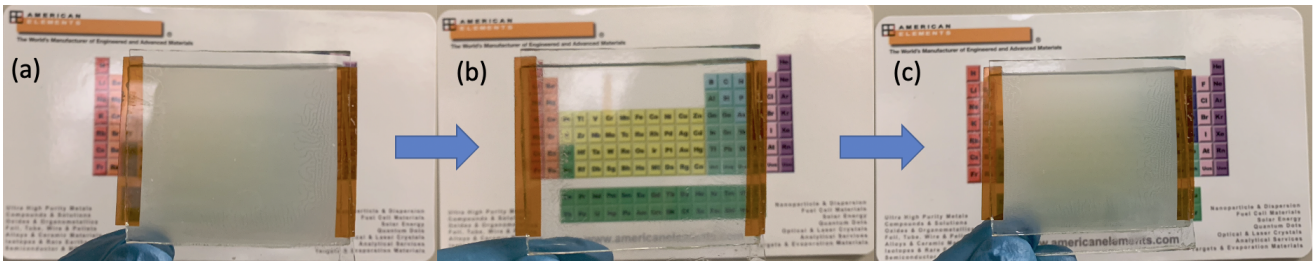

Figure 2-12. Demonstration of smart window film performance. From (a) to (c), a full cycle of a smart window is displayed, from (a) initial opaque film to (b) heated transparent state, then to (c) recovered opaque state.

2.3 Comparison of smart window films prepared with different solvents

The monomers of SA and ETPTA do not dissolve into each other, hence are unable to form a uniform opaque mixture after curing. A solvent is necessary to limit the phase separation to the micron level. The components co-dissolve in the solvent to render a clear uniform mixture, resulting in homogeneous smart window film. The added solvent should not evaporate too fast to create vacancies in films, and also not too slow to hinder the crystallization process. The volume of solvent added varies with the solvent type but should be optimized to an amount that the mixture is clear only at around 80~100°C. Too much solvent would also result in crystallization difficulties, causing a decrease in film opacity. In this section, films prepared with different solvents are characterized and compared for their properties.

2.3.1 Surface characterization

Smart window films prepared with acetone, methyl ethyl ketone (MEK), and ethanol are examined with an optical microscope as a comparison to pure SA film. In the optical images shown in Figure 2-13, the smart window films with two acrylate components all have clearer micro-sized patterns compared to neat SA film. However, due to the higher evaporation rate of acetone compared to MEK and ethanol, the last two samples showed better surface uniformity. Samples prepared with acetone usually have cavities due to acetone evaporation during the curing process. The amount of solvent used to dissolve 2 grams of smart window mixture decreases from acetone (760 μL) to MEK (480 μL) and then to ethanol (380 μL), indicating increasing dissolving ability and ethanol being the best solvent among these three. The surface phase separation pattern still exists, but since it was generated due to a more homogeneous mixture of SA and ETPTA moieties shows a smaller feature size.

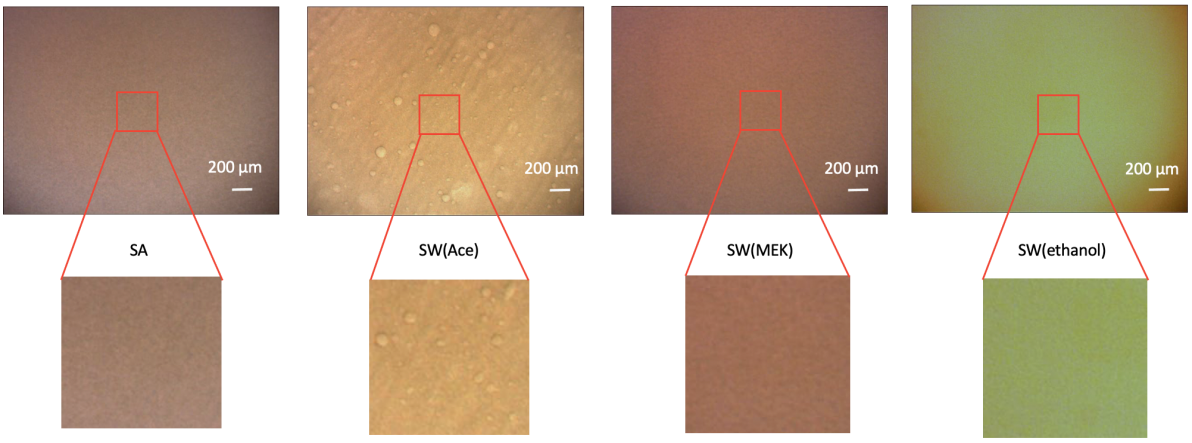

Figure 2-13. Optical images for neat SA film, SW prepared with acetone (760 µL/2g), MEK (480 µL/2g) and ethanol (380 µL/2g).

2.3.2 Results on transmittance and reflectance characterization

The parallel transmission spectra of smart window film samples made with pure SA, SW that used acetone, ethanol, and MEK as a solvent in the visible light range are also compared in Figure 2-14 (a). The transmittance differences here are obtained by comparing the transmittance of the samples at 550 nm in the spectrum. Dotted lines represent the transmittance of the films at a transparent state while solid lines are transmittance at an opaque state. The transmittance is sometimes greater than 100% because the reference here is double glass slides with spacers of 170 µm. Neat SA film with order crystalline structure has a strong preference for scattering light with a shorter wavelength, this is reflected in this graph where SA shows larger differences in transmittance with other samples in the region with longer wavelength, and the smart window films with two components have shown better shielding effect for visible light at opaque state. Correspondingly, the SA sample presented the highest transparency at a heated state and has shown a transmittance difference of 18.8%, 12.2%, and 7.3% with acetone, MEK, and ethanol,

respectively. However, due to the higher transmittance of pure SA film at room temperature, the smart window films still have a larger modulation range over the visible light region. Acetone, MEK, and ethanol have transmittance modulation ranges of 78.0%, 86.0%, and 96.8%.

To investigate how the type of solvent used is relevant to the transmission modulation, more samples were prepared with MEK and ethanol and the parallel transmission are compared in Figure 2-14 (b) and (c). (b) presented the transmittance of samples using ethanol as the solvent, 2-14 (c) presented the transmittance of samples using ethanol as the solvent. Here dotted lines represent measured transmittance after solvent evaporation. Solid lines are film transmittance measured right after the curing process and dotted lines represent corresponding measured transmittance after solvent evaporation. There was a gap of at least 24 hours between the first and second measurements. The transmittances of samples were measured right after the curing process, then one side of the glass was removed and left in the air for more than 24 hours to ensure complete evaporation of the solvent. Transmittance increases after solvent evaporation for both MEK and ethanol samples. These samples all experienced a 0~3% increase in transmittance at 550 nm. The increase in ΔT for ethanol samples are 1.8%, 2.5%, 2.4% and 0.6% while ΔT increases for MEK samples are 2.3%, 1.4% 1.6% and 1.3%. The smart window films, regardless of the solvent type, possessed good light-shielding characteristics. However, at 550 nm, the average measured transmittance before and after solvent evaporation for ethanol samples is 2.9% and 4.7% and MEK samples are 8.6% and 10.2%, ethanol still seems to be the better choice for solvent purposes.

The solvent amount can also affect light-transmitting properties. Films prepared with MEK were tested for visible light range parallel transmittance. For 2 grams of smart window film precursor, 440~540 μL of solvent was used (17.7~21.7% weight percentage) in dissolving

the mixture, and the results are presented in Figure 2-14 (d). From 440~500 μL, the transmittance only drops slightly (at 550 nm, 9.3% for 440 μL sample, 7.3% for 500 μL sample, but too much solvent (540 μL) that cannot evaporate during the curing process would hinder the formation of the crosslinking network consisting of the two components, resulting in a decrease in film opacity (15.2% at 550 nm). Within a certain range, 440~500 μL in the case of MEK, more solvent gave a more uniformly mixed blend of the two acrylates and resulted in better light shielding effect.

The relation of thickness and transmittance was investigated through three MEK samples prepared with thicknesses of 90 μm, 170 μm, and 260 μm, and results are displayed in Figure 2-14 (e). Transmittance decreases as thickness increases. Taking 550 nm to compare the transmittance for the samples, at opaque state, the 260 μm film provides the best shielding effect among the three samples (4.1%) but also shows a notable decrease in transmittance at transparent state (72.1%). The 90 μm film does not block visible light when heated but is also visibly more transparent (17.480%) at room temperature, compared to the two thicker samples. Transmittance modulation ranges at 550 nm from thinnest to thickest are 87.8%, 86.7%, and 68.0%, respectively. Considering the need for opacity and transparency at different states, the 170 μm film is the best choice for smart window film.

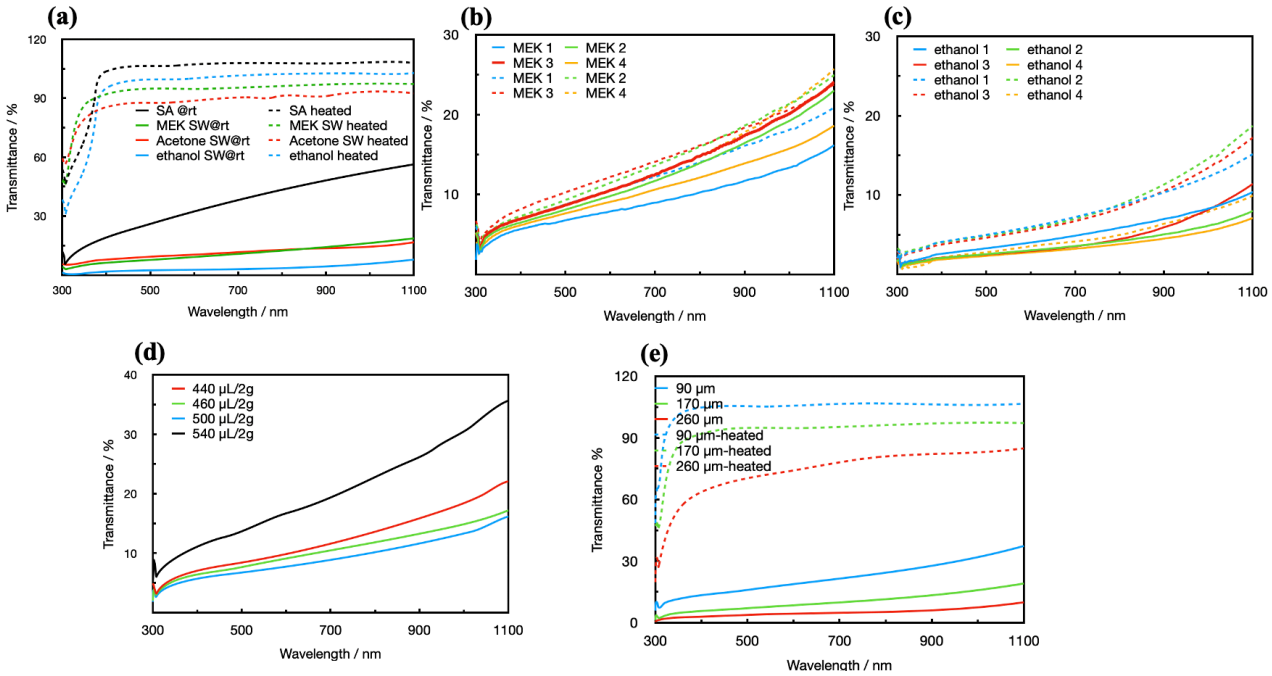

Figure 2-14. Transmission spectra for the smart window films. (a) Parallel transmission spectrum of smart window film samples made with pure SA, SW that used acetone, ethanol, and MEK as solvent. Parallel transmittance of samples using MEK (b) and ethanol (c) as the solvent. (d) Parallel transmission spectrum for samples prepared with various amounts of solvent (MEK). (e) Parallel transmission spectrum for samples prepared with MEK that have various thicknesses.

Film total reflectance was measured using a UV-VIS-NIR spectrophotometer with an integrating sphere, and the measuring mechanism is shown in Figure 2-15. The measurement light S hits the measuring face at an 8° incident angle. Baseline correction is performed with two standard plates, with one of the plates placed at the reflection position, and the measurement light enters the aperture and passes through the inside of the integrating sphere. The reflectance measured in this way is thus 100% reflectance. Sample reflectance is then measured as relative reflectance when the plate directly facing S is replaced by the film. If the sample is facing the

measurement light directly (0°), the specular reflectance factor would leave the sphere from the entrance. When the sample faces measurement light at an 8° angle, both specular and diffuse components in reflectance can be collected so total reflectance is measured.

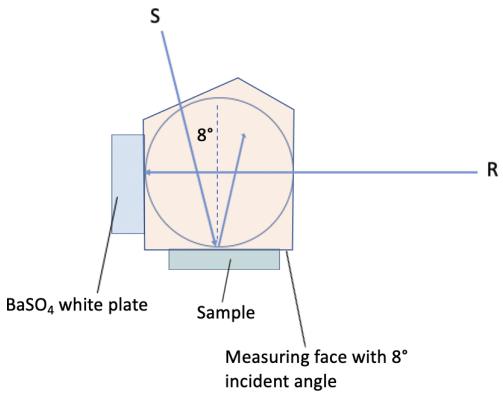

Figure 2-15. Total reflectance measurement illustration.

Transmittance and reflectance of films that used 170 μm spacers and 1 mm spacers were measured and compared in Figure 2-16. For the thinner sample (170 μm spacers), it was attached with one glass side during the measurement process. For transmittance measurement, the baseline was set on one glass slide, so transmittance was obtained for the film itself. For reflectance measurement, glass reflectance was measured first and compared with a reflectance of film+glass. For the thicker sample (1 mm spacers), no reference was attached, transmittance and reflectance were directly measured.

The ethanol film sample using 170 μm spacers showed a similar trend with MEK films in terms of transmittance: High diffusive transmittance at cold state (75.6% at 550 nm), high parallel transmittance at hot state (94.7% at 1500 nm), and a reduction in parallel transmittance when thickness increases. While the thin sample maintains an 11.2% parallel transmittance at 550 nm, the 1 mm film has close to zero transmittance in the same region, almost blocking

parallel transmission completely. The thick sample also has a stronger light scattering effect, illustrated in the diffusive transmittance spectrum. Scattering ability is weakened for the thinner film from a shorter wavelength to a longer wavelength; while for the thicker film, diffusive transmittance is maintained at around 50% until 1700 nm and decreases to 30~40% transmittance in the longer wavelength region. Total reflection of the two samples was also measured and presented in (b) and (d). The thinner film attached to glass has a reflection rate of up to 20%, while the thicker film, as a free-standing film, has over 30% reflection in the visible region by itself. In the NIR region, the reflection is still around 10%.

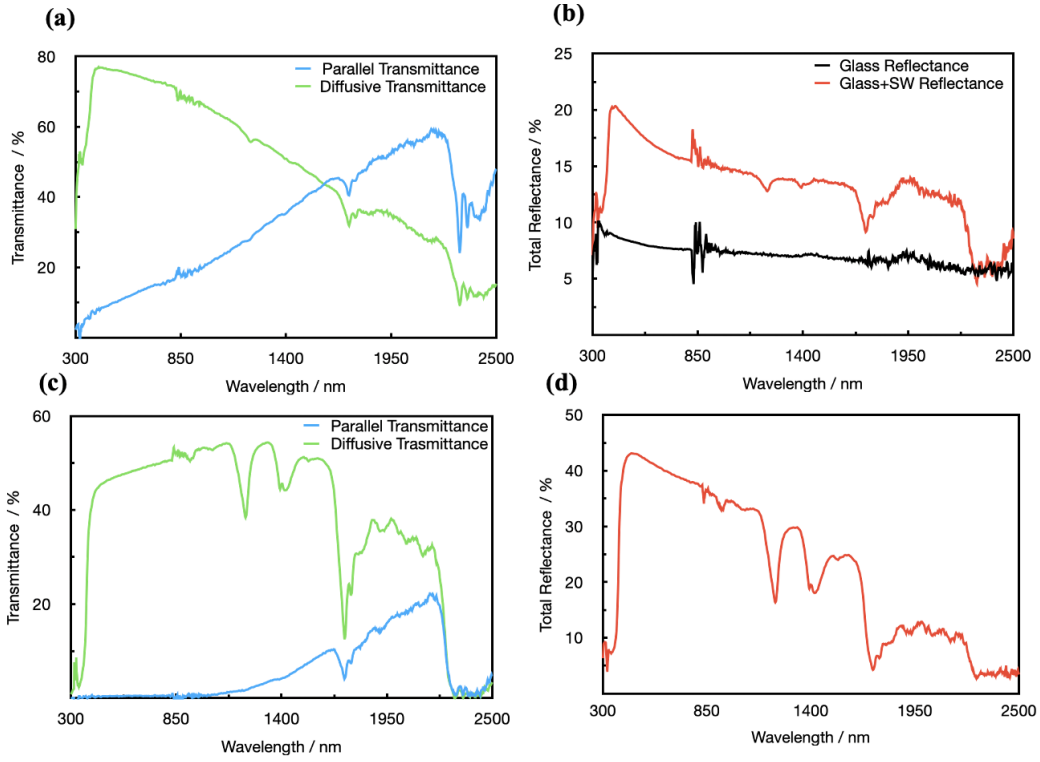

Figure 2-16. Transmittance and reflectance of ethanol film samples for visible and near-infrared regions. The graphs on the top are (a) transmittance and (b) reflectance graphs of a film sample using 170 μm spacers. The graphs at the bottom are (c) transmittance and (d) reflectance of the film sample using a 1mm thickness spacer.

Transmittance modulation of the 170 μm sample is also obtained using the equation in section 2.2.2 for solar, luminous and infrared regions. The overall solar modulation is 68.8%, while the visible light and IR modulations are 84.1% and 62.2%, respectively. Compared to MEK samples, the luminous modulation range improved by 13.2% and IR modulation decreased by 5.9%, therefore overall solar spectrum modulation slightly decreased by 2.6%. The integral reflectance of the 1 mm film was also calculated and gives 34.4%, 41.3%, 28.6% for solar, luminous, and IR regions. Combining with the transmittance modulation, the film is effective in terms of both privacy protection and heat shielding.

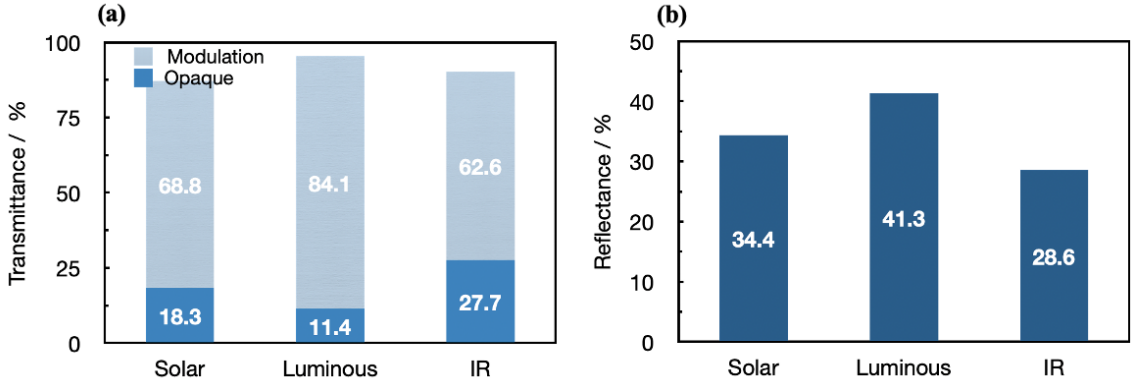

Figure 2-17. Transmittance modulation of the 170 μm sample (a) and integral total reflectance of the 1 mm thickness sample (b) for the solar, luminous, and infrared region.

2.3.3 Reversibility test and demonstration of transition process

A smart window film with ethanol as the solvent was also tested for cycling capability by measuring parallel transmittance at 550 nm, and after 50 cycles, the film was able to maintain the same level of opacity (average transmittance 3.2%) and transparency (average transmittance 101.0%) at two states, created 97.8% visible light modulation.

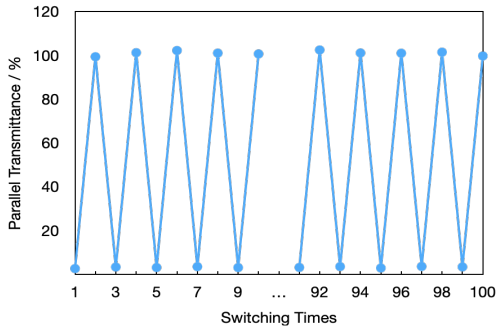

Figure 2-18. Cycling test for the smart window prepared with ethanol for 50 cycles. Parallel transmittance measured at 550 nm by the Shimadzu UV-1700 Pharmaspec spectrophotometer.

The demonstration of an ethanol smart window film (1 mm thickness) is presented in Figure 2-19. The film was placed directly on the paper and one side of the glass was removed. At opaque state, the "UCLA" pattern was completely blocked by the film and after heating up the film, the pattern was clearly displayed, indicating the film has high visual transparency even when thickness increased.

Figure 2-19. The demonstration of a complete transition process of a 1 mm thickness smart window film used ethanol as the solvent.

2.4 Chapter Summary

The properties of thermochromic smart window film are studied in this section. Pure poly stearyl acrylate film experiences semicrystalline-amorphous phase transition but only has nano-level crystal sizes that favor scattering visible light with short wavelengths (Rayleigh scattering). As a comparison, a smart window film with two components shows improved performance in light scattering due to the phase separation between the two acrylates enlarges the amorphous region in the resulting polymer. At ambient temperature, the semicrystalline structure of the crosslinking polymers effectively scatters both visible light and infrared, giving smart window film better shielding ability in the entire solar region. The film experiences phase change when heated, demonstrates high visual and infrared transparency at its transparent state, and is able to regain opacity when cooled down. The fabricated smart window film can reach a 71.4% overall solar spectrum modulation, 70.9% modulation visible region, and 68.5% modulation in the IR region. The difference between the transmittance at the heated transparent state and an opaque state indicating the film possesses good modulation ability and cycling durability over time.

Solvent affects the film's uniformity and therefore resulted in a difference in light-shielding ability. Acetone creates defects on the surface due to its fast evaporation during the curing process. MEK was used as a solvent to produce films that have a micro-level of phase separation between the two components that can scatter light effectively. Similar outcomes can be observed on films fabricated using ethanol as the solvent, with an improvement in light-blocking at the opaque state due to ethanol's better dissolving ability. A film with 1 mm thickness was then tested for transmittance and reflectance: the results showed that it blocks all parallel transmission in the visible region, and it can effectively reflect visible light (41.3%) and IR (28.6%).

Chapter 3 Fabrication of Transparent Silver Nanowire Heater

To use the thermochromic material as a smart window that can be easily and actively controlled, the device requires a transparent heater that can carry current and heat up the thermochromic layer through joule heating. Typically, ITO-coated transparent conducting glass is used extensively as the transparent conducting electrode in photovoltaic cells, organic light-emitting devices (OLEDs), and displays because of its high transparency (~90%) and conductance (10 Ω sq^{-1}). [76] However, the scarcity of ITO leads to its rising price and hence unsuitable for mass production, and its brittleness has made it inadequate for applications that need some degree of flexibility. Other metal oxides such as group III elements Al and Ga doped ZnO have been used as alternative transparent conducting oxides. [77] Carbon nanostructures-based heaters, such as single-walled nanotubes (SWNT) and multi-walled nanotubes (MWNT), possessed moderate transmittance and higher flexibility, however, its application in real-world settings still requires further development. [78] Metal nanowires and metal mesh both have high electrical conductivity at lower input voltages, but the metal mesh is created through lithography and that limits the area to only a few square centimeter areas since lithography processes are costly. [79] Among all the metals, silver has both the highest electrical conductivity and thermal conductivity and thus is considered to be one of the best choices for preparing transparent heaters.

Smart window applications need a simple device structure and easy operation. In order to supply energy to the smart window film, a transparent heater is needed. In this research, silver nanowires (AgNWs) embedded in polyurethane acrylate (PUA) film form the composite transparent heaters that supplied energy for the crystalline-to-amorphous transition through joule heating. Applying voltage to the heater generated heat that supplied energy for the phase

separation. The PUA film is selected because of its transparency, flexibility, and compatibility with the smart window layer. In terms of response time, applied power, and achieved temperature, a self-standing heater without supporting substrate can provide superb heating performance. A flexible and highly conductive heater is therefore produced from the combination of AgNW as the conductive material embedded in a transparent polymer matrix, both chemically and mechanically stable. [80]

The essential part of heater fabrication is to coat a uniformly interconnected AgNW network on the substrate to obtain a homogeneous heating effect. Solution-processed AgNWs are deposited using several techniques such as drop-casting, vacuum filtration, spray coating, and Meyer rod coating. [81] Here, Meyer rod coating is used to fabricate the transparent heaters for smart window devices.

The resistance of the metal network can be tuned by varying the nanowire density. The optical and electrical properties of AgNW are examined in this section, as well as the infrared properties and their dependence on the nanowire coverage rate. The thermal performance, including heating efficiency and thermal stability, is then investigated.

3.1 AgNW/PUA heater fabrication

3.1.1 Materials

Polyurethane acrylate (CN9009) and difunctional acrylic monomer (SR306) were supplied by Sartomer. Silver nanowires suspended in isopropanol (IPA) with an average diameter of 25~35 nm and an average length of 10~20 μm were supplied by Kechuang. The base mixture contains 1-Butanol by Fisher Scientific, dimethylformamide (DMF) by Sigma Aldrich, and IPA.

3.1.2 AgNW coating and fabrication

The as-purchased AgNW suspension dispersed in IPA was first centrifuged for 10 minutes at 3000 rpm to remove the impurities. After re-dissolve in the base mixture (5 mL 1-Butanol, 1 mL DMF, 3.75 mL IPA, and 0.25 mL H_2O in 10 mL mixture), 20 minutes vortex to re-disperse AgNW evenly in the mixture, followed by filtration to remove the nanowire agglomeration. The concentration was controlled to be around 1mg/mL to avoid aggregation of nanowires on the substrate surface.

A Meyor bar (RD Specialist) was used to coat AgNW on pre-cleaned glass slides as Figure 3-1 shows. Each glass slide has an area of 7.5×1.5 cm^2 and is oxygen-plasma treated for 30 minutes before coating. A setup in Figure 3-1 (including 6 glass slides on the top and 2 at the bottom) was fixed onto the bench surface; each blue rectangle in the graph indicates one glass slide. To coat each slide, 60 μL of AgNW solution was dripped on the end of the vertical glass slides in the setup. Then gentle force was applied on the Meyor bar to allow it to roll from top to bottom across the entire glass slide with slow and constant speed. After vaporization of the solvent, the coating process was repeated again and each time the top and bottom sides were flipped to ensure uniform distribution of nanowires. The coating process was repeated several times until the resistance reached an appropriate range. After coating, the coated glass slides were treated with annealing at 80°C for 10 minutes to stabilize the nanowire network structure.

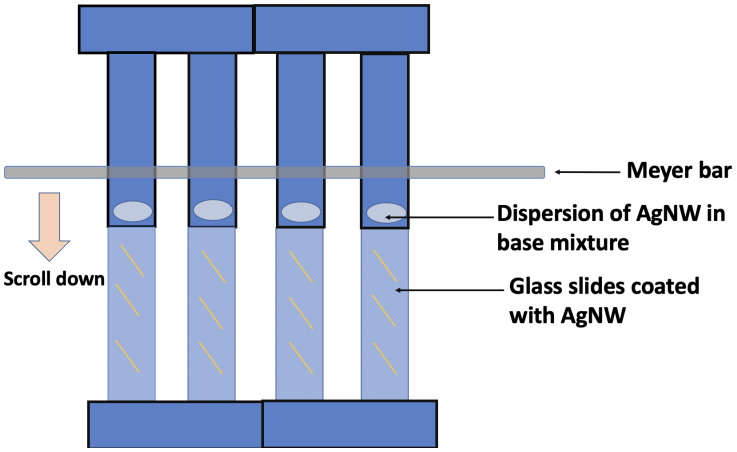

Figure 3-1. Illustration of AgNW coating process.

3.1.3 Fabrication of transparent heater

The Meyer bar coating AgNW process is demonstrated in Figure 3-2. CN9009 and SR306 were mixed with a weight ratio of 3:1 to give the PUA precursor. 1 wt% of DMPA was added as a photo-initiator, followed by 3-hour ultrasonication to get a uniform solution. The AgNW-coated glass slide and a clean one separated by 90 μm thickness tape were fixed at short ends and pre-heated at 120°C for 5 minutes on the hot plate, along with the obtained PUA precursor which has high viscosity. The precursor was injected into space between glass slides and cured under UV for 3 minutes. Then the glass slides were carefully peeled off, leaving a free-standing AgNW/PUA composite film. In order to test the heating performance of the transparent heater, copper wires were fixed at the film's short ends with silver paste and tapes and then connected to the DC power source.

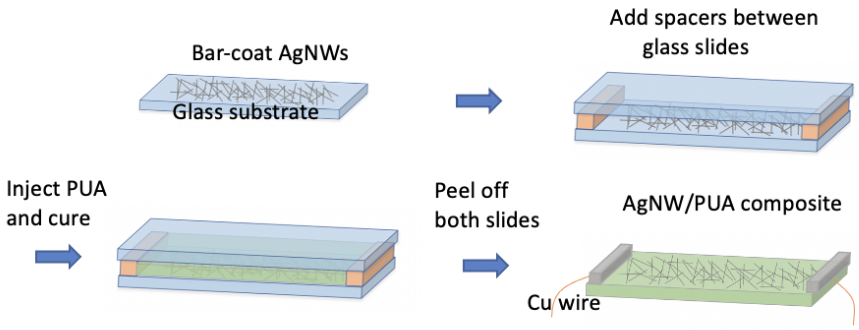

Figure 3-2. The fabrication process of the transparent heater. PUA precursor is injected into space between two glass slides (one is coated with AgNW) separated by 90 μm thickness spacers and cured under UV light for three minutes.

3.1.4 Characterization

Transmittance in visible light (300~800 nm) and NIR range (800~2500 nm) measured by Shimadzu ISR-3100 UV-VIS-NIR spectrophotometer with integrating sphere. The temperature was recorded every second using a TC-08 thermocouple data logger. The DC power source used was Agilent E3621A DC power supply, and heating voltage and current can be adjusted.

3.2 Transmittance of AgNW network

To achieve the best heating performance, AgNWs need to form a uniformly distributed network on the glass slide to create a smooth pathway for electrons. The fabrication process techniques and substrate type can both pose an influence on the heater sheet resistance, affecting the final heating performance.

AgNW is randomly distributed on the surface of glass slides after coating. Annealing was then applied on AgNW coated glass slides. The overlapping of AgNW would cause problems in

supplying heat uniformly to the phase separation layer, thus annealing is crucial to maintain its function. Annealing helps to stabilize the structure for further application by reducing the crossing of the AgNW and hence reduces AgNW's resistance. To study AgNW's shielding effect depending on density, four sample heaters with different sheet resistance, 10 Ω sq^{-1}, 15 Ω sq^{-1}, 20 Ω sq^{-1}, 25 Ω sq^{-1}, were coated and compared. Resistance slightly dropped after annealing and again experienced a decrease when AgNWs were transferred from glass slides to PUA film, becoming 8.8 Ω sq^{-1}, 12.3 Ω sq^{-1}, 19.3 Ω sq^{-1}, and 22.5 Ω sq^{-1}. The coated AgNW layer was then transferred to the PUA matrix since PUA protects the AgNW network from the surrounding environment.

The parallel transmission spectra are displayed in Figure 3-3. For AgNW deposited on glass slides (Figure 3-3(a)), transmittances at 550 nm decrease as sheet resistance increases, are 81.0%, 86.3%, 89.7% and 92.1%, respectively. Compared to the neat PUA film that has 100% transmission at 550 nm, the transmittances for AgNW/PUA composite become 76.6%, 82.0%, 91.4%, and 92.0%, respectively (Figure 3-3(b)). The two AgNWs composite heaters with higher resistance (20 Ω sq^{-1}, 25 Ω sq^{-1}) have over 90% transmittance, providing good visual transparency.

The total and diffusive transmittance including both visible and infrared regions were measured with a UV-VIS-NIR spectrometer (Figure 3-3 c-d). Total transmittance shows a similar trend as the parallel transmittance in the visible light range (300~800 nm), decreases slightly as resistance increases. In the near-infrared range, the heater samples' IR-shielding ability show larger differences. Pure PUA film still has a high transmittance, AgNWs block NIR leads to a distinct drop in transmittance. On the other hand, the thin layer of AgNW has a limited effect on light scattering, only a very small proportion of visible light and NIR were scattered by

the transparent heater layer. There is also no notable variation between heaters with different resistances, which is reflected by the diffusive transmittance figure. Considering the practical usage of the transparent heater, AgNWs composites with a sheet resistance roughly of 20~25 Ω sq^{-1} were selected for achieving relatively good visual and NIR transparency that does not hinder the normal function of a smart window.

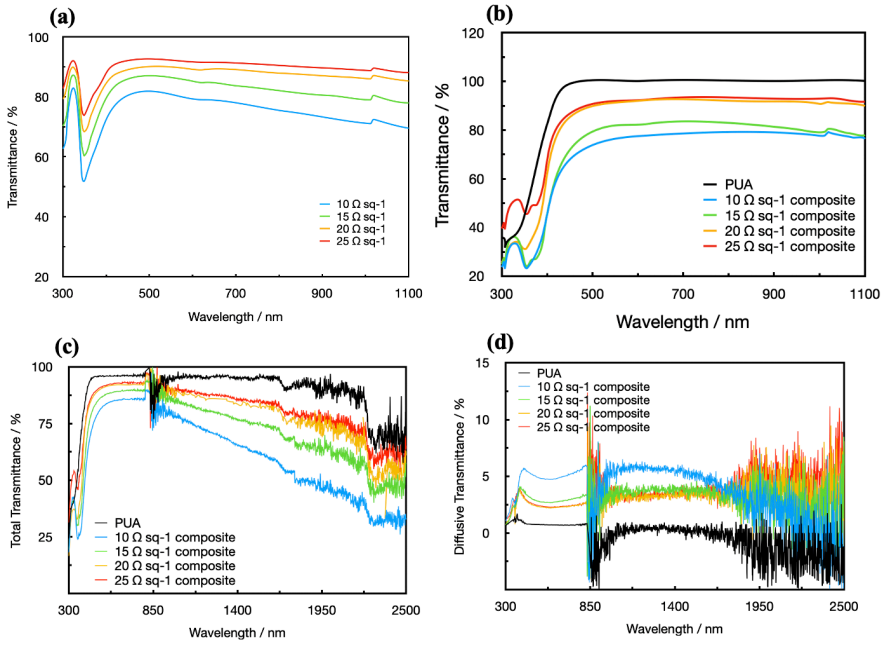

Figure 3-3. Transmittance performance of the AgNW/PUA composite heaters. Parallel transmittance spectrum of AgNW with different sheet resistance on glass (a) and on PUA(b). (c) Total transmittance and (d) Diffusive transmittance of samples in the visible light and NIR region.

3.3 Heating performance of the composite transparent heater

The heating performance of the transparent heater was evaluated by recording the surface temperature at every second of an AgNW/PUA composite film with a thickness of 170 μm and

sheet resistance of 7 Ω sq^{-1} using a thermocouple, and the performance diagrams are presented in Figure 3-4.

The saturation temperatures at each stage from 0~5V are displayed in Figure 3-4 (a). Starting from room temperature of 18.5 °C, the applied voltage at each level was kept for two minutes until the film temperature became stable. The heating stability of the heater was tested by applying voltage at a 5.3V for two hours, and from Figure 3-4 (b) it is observed that the surface temperature was maintained at around 60°C in the entire testing duration without large fluctuations, proving the long-term stability of the composite film as a heater in smart window device. Figure 3-4 (c) shows the fitted curve between the saturation temperature is directly proportional to the square of the applied DC voltage. The heating power is calculated by multiplying heating voltage and current, and its linear relationship with temperature is plotted in (d).

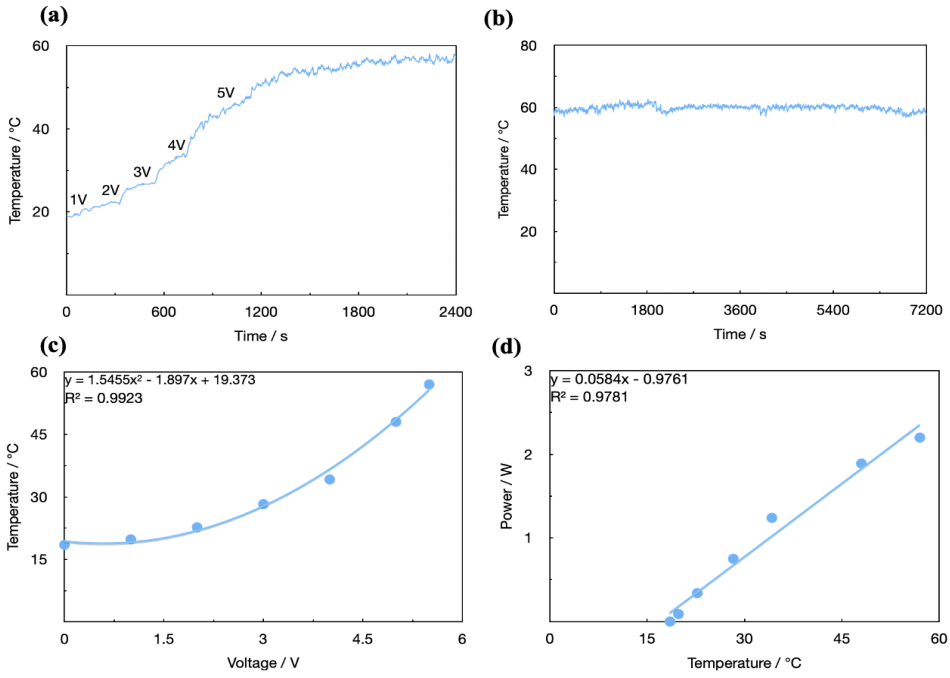

Figure 3-4. Heating performance graphs for the AgNW/PUA composite heaters. (a) The saturation temperature at an applied voltage from 1~5V. (b) The temperature of the heater recorded using a thermocouple for 2 hours at 5.3V applied voltage. (c) Heater saturation temperature as a function of applied voltage. (d) Heating power versus temperature.

3.4 Chapter Summary

In this section, the AgNW/PUA composite heater was fabricated, and its properties were investigated. The Ag nanowires were deposited onto the glass slide through the Meyer bar coating method, and then nanowires were transferred to PUA film to give a free-standing transparent heater. The resulting heater has shown good visual transparency, as well as long-term heating stability, therefore would serve as an appropriate candidate as the heater of a smart window device.

Chapter 4 Preparation and Optical Performance of Smart Window Device

The assembling process of a smart window includes sandwiching the phase-changing polymer film between a transparent heater and a PUA protection layer. The performance of the smart window device is also evaluated in this section.

4.1 Fabrication of a smart window device

The fabrication of a smart window device is displayed in three steps below, from Figure 4-1(a) to (c). First, the detailed Meyer bar coating AgNW process, followed by PUA precursor injection, is demonstrated in Figure 3-2. The same procedure was followed here but only removed one glass slide to expose the AgNW side to the air. This process is shown in Figure 4-1(a).

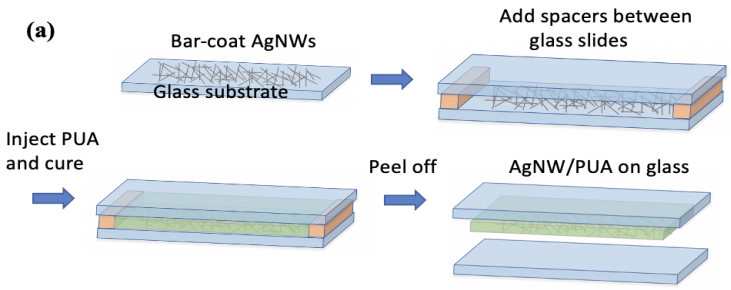

Figure 4-1(a) AgNW coating and composite heater fabrication process.

Another PUA protection layer was fabricated by injecting PUA precursor in between two glass slides separated by spacers (90 μm thickness tape) and cured under UV for 3 minutes, shown in Figure 4-1(b).

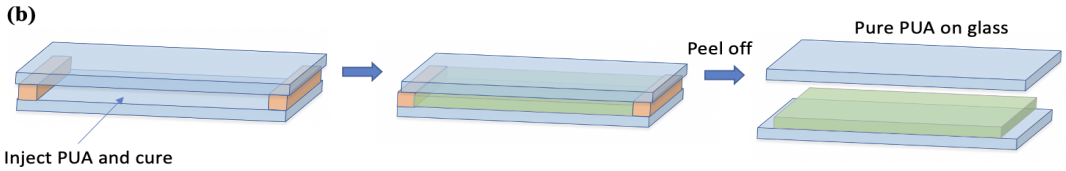

Figure 4-1(b). PUA protection layer fabrication.

The assembling process is illustrated in the next step, in Figure 4-1(c), where the transparent PUA film and AgNW composite heater were used to sandwich the smart window film. The final device with laminated structure was assembled by injecting the smart window precursor into the space between PUA film and AgNW/PUA heater that was separated by 170 μm thickness spacer, then UV cured for 3 minutes. After curing, the solvent of the precursor evaporated, leaving the thickness of the smart window film to be around 150 μm. Copper wires were fixed at both short ends by attached tape on the exposed AgNW, leaving an active heating area of around 6.5×1.5 cm^2. Silver paste was applied on the conjunction of tape, copper wire, and AgNW/PUA film to establish an electron pathway.

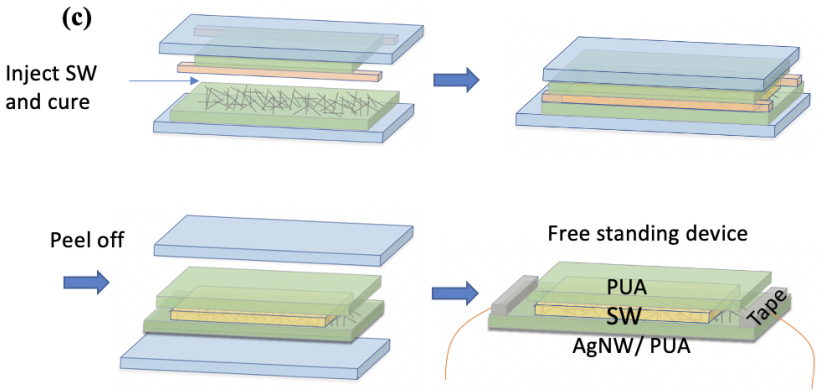

Figure 4-1(c). The process of smart window film fabrication and device assembling.

4.2 Smart window device demonstration

The assembled smart window can be assembled through the procedures displayed in Figure 4-1. A demonstration of a complete switching cycle is shown in Figure 4-2 (a): a smart window device was placed on a glass petri dish which was placed on a sheet of paper that has the "UCLA" pattern. There was a 1 cm distance between the film and paper. The underneath "UCLA" pattern was completely blocked by the smart window film at the initial state; when voltage was applied, the film was heated up and quickly switched to a transparent state, revealing the paper pattern. The transparent film was restored to its original opaque state after removing the power source and cooling down.

In Figure 4-2 (b), a complete transition is again displayed, but this time the device was attached to a curved beaker wall. The initial opaque device blocked the paper pattern behind the beaker and revealed the pattern when the temperature rose and the smart window film became transparent. After cooling down, the device returned to an opaque state. This indicated the smart window device is still functional at a surface with curvature, implying the device's potential in various scenarios.

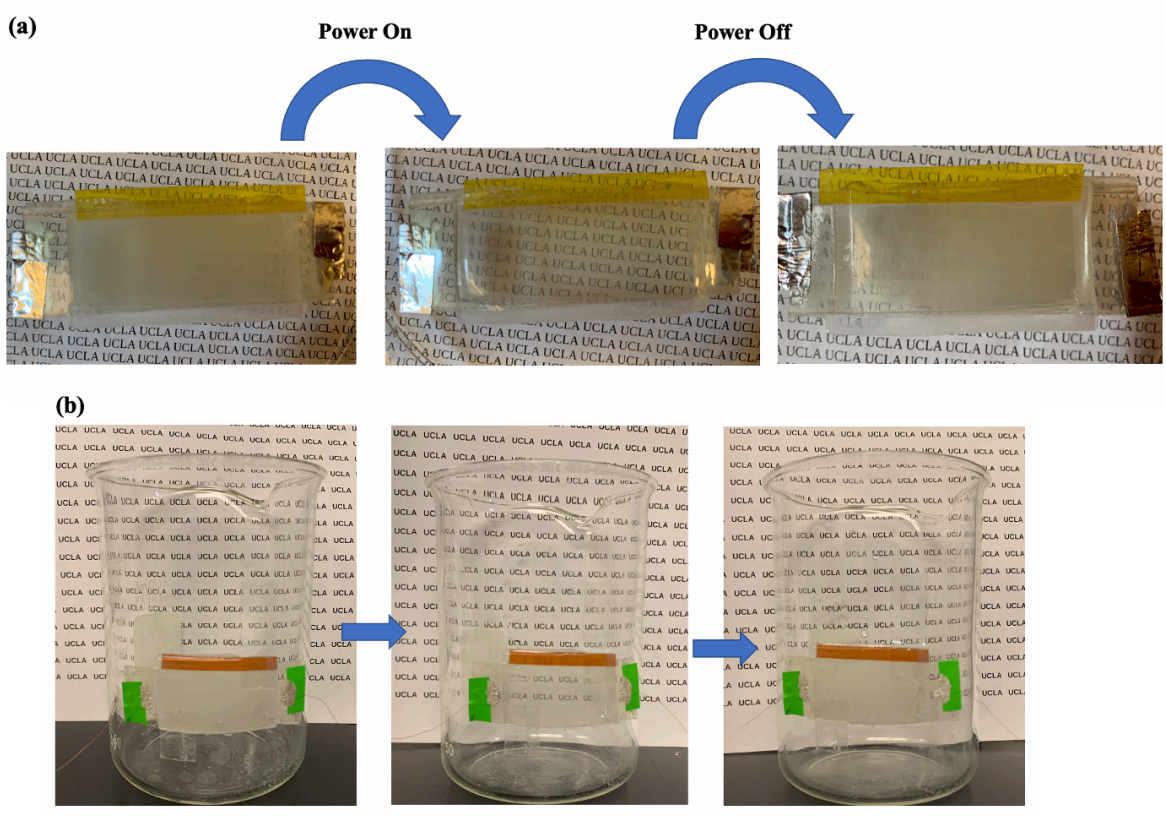

Figure 4-2. Smart window device demonstration. (a) Demonstration of a smart window device on visible light shielding at power on and power off states. (b). Demonstration of a complete opaque-transparent-opaque transition process of a curved assembled smart window device fixed on a beaker wall.

The transmittance of a smart window device assembled from a 23 Ω sq^{-1} composite heater (90 μm), PUA protection layer, and smart window layer (150 μm) was measured. The device at the opaque state and the transparent state presented 72.2% and 13.7% transmittance at 550 nm, 78.4%, and 32.4% at 1100 nm, resulting in 58.5% and 46.0% modulation range for visible and IR regions. The assembled device maintains the modulation ability of the smart

window film layer and can be switched between light-transmitting and light-shielding mode when applying power.

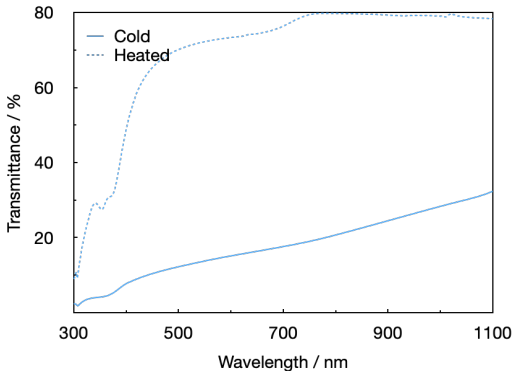

Figure 4-3. The transmittance of the smart window device. The device was assembled with a smart window film (150 μm thickness, prepared with MEK), an AgNW/PUA transparent heater (sheet resistance 23 Ω sq^{-1}, 90 μm thickness), and a PUA transparent protection layer (90 μm thickness).

4.3 Chapter Summary

A whole smart window device was assembled through three steps: first fabricated AgNW/PUA composite transparent heater, then the pure PUA protection layer and sandwiched the smart window film between the heater and PUA layer. By applying and removing DC power supply, the smart window device can be switched between opaque and transparent state. The device can also be attached to a curved surface, which gives it the possibility to be applied to various situations.

Chapter 5 Summary and Future Prospects

A thermochromic material was studied for smart window purposes in this thesis. The film utilizes the temperature-dependent phase transition property of poly stearyl acrylate and the micro-level phase separation between stearyl acrylate and ethoxylated trimethylolpropane triacrylate, in order to achieve Mie scattering that resulted in an increased film opacity at room temperature. At a cold state (room temperature), both visible light and infrared are scattered by the semicrystalline structure, giving the film an opaque appearance. When heated above the transition temperature, the film experiences a phase change and becomes highly transparent; but the film is still able to restore to its original opacity once it cools down. The fabricated film in this study was tested for solar modulation ability and has demonstrated 71.4% transmission modulation over the whole solar spectrum, 70.9% for the visible light modulation, and 68.5% for the infrared modulation. The film maintains modulation ability in both visible light and infrared regions, giving it an advantage compared to other potential thermochromic materials. The cycling capability was tested through monitoring transmittance changes during 50 cycles, and it was observed that the film maintained over 50% parallel transmittance difference and over 60% diffusive transmittance difference from the first to the last five cycles during switching.

Smart window films fabricated with different solvents also presented some differences in film properties. When ethanol was used as a solvent, film visible light shielding ability was improved because ethanol's better dissolving ability gives a homogeneous mixture of the two components. When the film thickness increases, visible light shielding property is further improved. The 1 mm thickness film can achieve ~0% luminous transmittance and 34.4% reflection rate for the solar spectrum at opaque state, effectively reducing unwanted heat transfer;

the film can switch to transparent state at elevated temperature to function as a traditional glass window.

The smart window film achieves opaque-to-transparent transition through joule heating. A transparent silver nanowire/PUA composite heater was fabricated, and it has been proven to be able to reach smart window transition temperature when connected to a DC power source while maintaining high visual transparency. The heater also has long-term stability, therefore is a feasible choice for a smart window heating component. A whole smart window device was then assembled with a pure PUA protection film, a smart window film, and a transparent composite heater. The device can be easily switched between light transmitting and light blocking mode by applying and removing the DC power source and remains functional when it is fixed to a curved surface. For further improvement, films might be studied for energy-saving analysis.

References

[1] Pérez-Lombard, L., Ortiz, J., & Pout, C. A review on buildings energy consumption information. *Energy and Buildings*, 2008, 40(3), 394-398.

[2] Zhao, H. X., & Magoulès, F. A review on the prediction of building energy consumption. *Renewable and Sustainable Energy Reviews*, 2012, 16(6), 3586-3592.

[3] Baetens R, Jelle B P, Gustavsen A. Properties, requirements and possibilities of smart windows for dynamic daylight and solar energy control in buildings: A state-of-the-art review[J]. *Solar Energy Materials and Solar Cells*, 2010, 94(2): 87-105.

[4] Rezaei, S. D., Shannigrahi, S., & Ramakrishna, S. A review of conventional, advanced, and smart glazing technologies and materials for improving indoor environment. *Solar Energy Materials and Solar Cells*, 2017, 159, 26-51.

[5] Lang, F., Wang, H., Zhang, S., Liu, J., & Yan, H. Review on variable emissivity materials and devices based on smart chromism. *International Journal of Thermophysics*, 2018, 39(1), 6.

[6] DeForest, N., Shehabi, A., O'Donnell, J., Garcia, G., Greenblatt, J., Lee, E. S., ... & Milliron, D. J. United States energy and CO2 savings potential from deployment of near-infrared electrochromic window glazings. *Building and Environment*, 2015, 89, 107-117.

[7] Wang, Y., Runnerstrom, E. L., & Milliron, D. J. Switchable materials for smart windows. *Annual Review of Chemical and Biomolecular Engineering*, 2016, 7, 283-304.

[8] Apte, J., & Arasteh, D. Window-related energy consumption in the US residential and commercial building stock, 2008.

[9] Casini, M. Active dynamic windows for buildings: A review. *Renewable Energy*, 2018, 119, 923-934.

[10] Ke, Y., Chen, J., Lin, G., Wang, S., Zhou, Y., Yin, J., ... & Long, Y. Smart Windows: Electro-, Thermo-, Mechano-, Photochromics, and Beyond. *Advanced Energy Materials*, 2019, 9(39), 1902066.

[11] Kamalisarvestani, M., Saidur, R., Mekhilef, S., & Javadi, F. S. Performance, materials and coating technologies of thermochromic thin films on smart windows. *Renewable and Sustainable Energy Reviews*, 2013, 26, 353-364.

[12] Cao, D., Xu, C., Lu, W., Qin, C., & Cheng, S. Sunlight-Driven Photo-Thermochromic Smart Windows. *Solar RRL*, 2018, 2(4), 1700219.

[13] Wang, L., Liu, Y., Zhan, X., Luo, D., & Sun, X. Photochromic transparent wood for photo-switchable smart window applications. *Journal of Materials Chemistry C*, 2019, 7(28), 8649-8654.

[14] Long, L., & Ye, H. How to be smart and energy efficient: A general discussion on thermochromic windows. *Scientific Reports*, 2014, 4, 6427.

[15] Kim, H. N., & Yang, S. Responsive Smart Windows from Nanoparticle–Polymer Composites. *Advanced Functional Materials*, 2019, 1902597.

[16] Ruhmann, R., Seeboth, A., Muehling, O., & Loetzsch, D. Thermotropic materials for adaptive solar control. In *Advances in Science and Technology* (Vol. 77, pp. 124-131), 2013. Trans Tech Publications Ltd.

[17] Orgiu, E., & Samori, P. 25th anniversary article: organic electronics marries photochromism: generation of multifunctional interfaces, materials, and devices. *Advanced Materials*, 2014, 26(12), 1827-1845.

[18] Pan, L., Wang, Y., Wang, X., Qu, H., Zhao, J., Li, Y., & Gavrilyuk, A. Hydrogen photochromism in Nb2O5 powders. *Physical Chemistry Chemical Physics*, 2014, 16(38), 20828-20833.

[19] Schrauben, J. N., Hayoun, R., Valdez, C. N., Braten, M., Fridley, L., & Mayer, J. M. Titanium and zinc oxide nanoparticles are proton-coupled electron transfer agents. *Science*, 2012, 336(6086), 1298-1301.

[20] Lee, H. Y., Cai, Y., Bi, S., Liang, Y. N., Song, Y., & Hu, X. M. A dual-responsive nanocomposite toward climate-adaptable solar modulation for energy-saving smart windows. *ACS Applied Materials & Interfaces*, 2017, 9(7), 6054-6063.

[21] Adachi, K., Tokushige, M., Omata, K., Yamazaki, S., & Iwadate, Y. Kinetics of coloration in photochromic tungsten (VI) oxide/silicon oxycarbide/silica hybrid xerogel: insight into cation self-diffusion mechanisms. *ACS Applied Materials & Interfaces*, 2016, 8(22), 14019-14028.

[22] Miyazaki, H., Ishigaki, T., & Ota, T. Photochromic smart windows employing WO3-based composite films. *Journal of Materials Science Research*, 2017, 6, 62.

[23] Zhang, S., Cao, S., Zhang, T., Fisher, A., & Lee, J. Y. Al 3+ intercalation/de-intercalation-enabled dual-band electrochromic smart windows with a high optical modulation, quick response and long cycle life. *Energy & Environmental Science*, 2018, 11(10), 2884-2892.

[24] Leinberg, S., Kisand, V., Šutka, A., Saal, K., Lõhmus, R., Joost, U., ... & Nõmmiste, E. Switchable optical transmittance of TiO2 submicron-diameter wire suspension-based "smart window" device. *Optical Materials*, 2015, 46, 418-422.

[25] Maeda, S., Fujita, M., Idota, N., Matsukawa, K., & Sugahara, Y. Preparation of transparent bulk TiO2/PMMA hybrids with improved refractive indices via an in situ polymerization process

using TiO2 nanoparticles bearing PMMA chains grown by surface-initiated atom transfer radical polymerization. *ACS Applied Materials & Interfaces*, 2016, 8(50), 34762-34769.

[26] Wu, W., Wang, M., Ma, J., Cao, Y., & Deng, Y. Electrochromic metal oxides: Recent progress and prospect. *Advanced Electronic Materials*, 2018, 4(8), 1800185.

[27] Cai, G., Cui, M., Kumar, V., Darmawan, P., Wang, J., Wang, X., ... & Lee, P. S. Ultra-large optical modulation of electrochromic porous WO 3 film and the local monitoring of redox activity. *Chemical Science*, 2016, 7(2), 1373-1382.

[28] Cao, S., Zhang, S., Zhang, T., Fisher, A., & Lee, J. Y. Metal-doped TiO2 colloidal nanocrystals with broadly tunable plasmon resonance absorption. *Journal of Materials Chemistry C*, 2018, 6(15), 4007-4014.

[29] Li, H., McRae, L., Firby, C. J., Al-Hussein, M., & Elezzabi, A. Y. Nanohybridization of molybdenum oxide with tungsten molybdenum oxide nanowires for solution-processed fully reversible switching of energy storing smart windows. *Nano Energy*, 2018, 47, 130-139.

[30] Thakur, V. K., Ding, G., Ma, J., Lee, P. S., & Lu, X. Hybrid materials and polymer electrolytes for electrochromic device applications. *Advanced Materials*, 2012, 24(30), 4071-4096.

[31] Cai, G., Eh, A. L. S., Ji, L., & Lee, P. S. Recent advances in electrochromic smart fenestration. *Advanced Sustainable Systems*, 2017, 1(12), 1700074.

[32] Li, C. C., Tseng, H. Y., Chen, C. W., Wang, C. T., Jau, H. C., Wu, Y. C., ... & Lin, T. H. (2018, May). 43-1: Tri-stable Cholesteric Liquid Crystal Smart Window. In *SID Symposium Digest of Technical Papers* (Vol. 49, No. 1, pp. 543-545).

[33] Choi, G. J., Jung, H. M., Lee, S. H., & Gwag, J. S. Infrared shutter using cholesteric liquid crystal. *Applied Optics*, 2016, 55(16), 4436-4440.

[34] Oh, S. W., Baek, J. M., Heo, J., & Yoon, T. H. Dye-doped cholesteric liquid crystal light shutter with a polymer-dispersed liquid crystal film. *Dyes and Pigments*, 2016, 134, 36-40.

[35] Lan, Z., Li, Y., Dai, H., & Luo, D. Bistable smart window based on ionic liquid doped cholesteric liquid crystal. *IEEE Photonics Journal*, 2017, 9(1), 1-7.

[36] Huh, J. W., Choi, T. H., Woo, J. H., Kim, J. H., Do, S. M., Seo, J. H., & Yoon, T. H. Bistable liquid-crystal phase grating device for smart window and window display applications. In *Emerging Liquid Crystal Technologies XV* (2020, February, Vol. 11303, p. 113030J). International Society for Optics and Photonics.

[37] Khandelwal, H., Schenning, A. P., & Debije, M. G. Infrared regulating smart window based on organic materials. *Advanced Energy Materials*, 2017, 7(14), 1602209.

[38] Leung, E. M., Escobar, M. C., Stiubianu, G. T., Jim, S. R., Vyatskikh, A. L., Feng, Z., ... & Karshalev, E. A dynamic thermoregulatory material inspired by squid skin. *Nature Communications*, 2019, 10(1), 1-10.

[39] Zhu, Y., Antao, D. S., Xiao, R., & Wang, E. N. Real-Time Manipulation with Magnetically Tunable Structures. *Advanced Materials*, 2014, 26(37), 6442-6446.

[40] Li, Z., Zhai, Y., Wang, Y., Wendland, G. M., Yin, X., & Xiao, J. Harnessing surface wrinkling–cracking patterns for tunable optical transmittance. *Advanced Optical Materials*, 2017, 5(19), 1700425.

[41] Zhang, R., Wang, Q., & Zheng, X. Flexible mechanochromic photonic crystals: routes to visual sensors and their mechanical properties. *Journal of Materials Chemistry C*, 2018, 6(13), 3182-3199.

[42] Xu, C., Stiubianu, G. T., & Gorodetsky, A. A. Adaptive infrared-reflecting systems inspired by cephalopods. *Science*, 2018, 359(6383), 1495-1500.

[43] Kim, H. N., Ge, D., Lee, E., & Yang, S. Multistate and On-Demand Smart Windows. *Advanced Materials*, 2018, 30(43), 1803847.

[44] Wang, X., Li, M., Wang, D., Zhang, H., Duan, R., Zhang, D., ... & Dong, B.. Low-Cost, Robust Pressure-Responsive Smart Windows with Dynamic Switchable Transmittance. ACS *Applied Materials & Interfaces*, 2020, 12(13), 15695-15702.

[45] Phan, L., Kautz, R., Leung, E. M., Naughton, K. L., Van Dyke, Y., & Gorodetsky, A. A. Dynamic materials inspired by cephalopods. *Chemistry of Materials*, 2016, 28(19), 6804-6816.

[46] https://www.commercialwindows.org/dynamic.php (accessed:June 2020).

[47] Ke, Y., Zhou, C., Zhou, Y., Wang, S., Chan, S. H., & Long, Y. Emerging thermal-responsive materials and integrated techniques targeting the energy-efficient smart window application. *Advanced Functional Materials*, 2018, 28(22), 1800113.

[48] Zhang, J., Wang, J., Yang, C., Jia, H., Cui, X., Zhao, S., & Xu, Y. Mesoporous SiO2/VO2 double-layer thermochromic coating with improved visible transmittance for smart window. *Solar Energy Materials and Solar Cells*, 2017, 162, 134-141.

[49] Ji, C., Wu, Z., Wu, X., Wang, J., Gou, J., Huang, Z., ... & Jiang, Y. Al-doped VO2 films as smart window coatings: reduced phase transition temperature and improved thermochromic performance. *Solar Energy Materials and Solar Cells*, 2018, 176, 174-180.

[50] Kang, L., Gao, Y., Luo, H., Chen, Z., Du, J., & Zhang, Z. Nanoporous thermochromic VO2 films with low optical constants, enhanced luminous transmittance and thermochromic properties. *ACS Applied Materials & Interfaces*, 2011, 3(2), 135-138.

[51] Ren, H., Hassna, O., Li, J., & Arigong, B. A patterned phase-changing vanadium dioxide film stacking with VO2 nanoparticle matrix for high performance energy-efficient smart window applications. *Applied Physics Letters*, 2021, 118(5), 051901.

[52] Zhao, Z., Liu, Y., Yu, Z., Ling, C., Li, J., Zhao, Y., & Jin, H. Sn–W Co-doping Improves Thermochromic Performance of VO2 Films for Smart Windows. *ACS Applied Energy Materials*, 2020, 3(10), 9972-9979.

[53] Fang, Z., Tian, S., Li, B., Liu, Q., Liu, B., Zhao, X., & Sankar, G. VO2/ZnO bilayer films with enhanced thermochromic property and durability for smart windows. *Applied Surface Science*, 2021, 540, 148414.

[54] Wang, Y., Zhao, F., Wang, J., Khan, A. R., Shi, Y., Chen, Z., ... & Guo, X. VO2@ SiO2/Poly (N-isopropylacrylamide) hybrid nanothermochromic microgels for smart window. *Industrial & Engineering Chemistry Research*, 2018, 57(38), 12801-12808.

[55] Ke, Y., Yin, Y., Zhang, Q., Tan, Y., Hu, P., Wang, S., ... & White, T. J. Adaptive thermochromic windows from active plasmonic elastomers. *Joule*, 2019, 3(3), 858-871.

[56] Seeboth, A., Kriwanek, J., Lötzsch, D., & Patzak, A. Chromogenic polymer gels for reversible transparency and color control with temperature at a constant volume. *Polymers for Advanced Technologies*, 2002, 13(7), 507-512.

[57] Zhou, Y., Dong, X., Mi, Y., Fan, F., Xu, Q., Zhao, H., ... & Long, Y. Hydrogel smart windows. *Journal of Materials Chemistry A*, 2020, 8(20), 10007-10025.

[58] Zhou, Y., Cai, Y., Hu, X., & Long, Y. Temperature-responsive hydrogel with ultra-large solar modulation and high luminous transmission for “smart window” applications. *Journal of Materials Chemistry A*, 2014, 2(33), 13550-13555.

[59] Owusu-Nkwantabisah, S., Gillmor, J., Switalski, S., Mis, M. R., Bennett, G., Moody, R., ... & Slater, G. Synergistic thermoresponsive optical properties of a composite self-healing hydrogel. *Macromolecules*, 2017, 50(9), 3671-3679.

[60] Zhou, Y., Layani, M., Wang, S., Hu, P., Ke, Y., Magdassi, S., & Long, Y. Fully printed flexible smart hybrid hydrogels. *Advanced Functional Materials*, 2018, 28(9), 1705365.

[61] Lee, H. Y., Cai, Y., Bi, S., Liang, Y. N., Song, Y., & Hu, X. M. A dual-responsive nanocomposite toward climate-adaptable solar modulation for energy-saving smart windows. *ACS Applied Materials & Interfaces*, 2017, 9(7), 6054-6063.

[62] Nitz, P., & Hartwig, H. Solar control with thermotropic layers. *Solar Energy*, 2005, 79(6), 573-582.

[63] Byker, H. J., Millett, F. A., & Ogburn, P. H. U.S. Patent No. 6,362,303. Washington, DC: U.S. Patent and Trademark Office, 2002.

[64] Wang, N., Magdassi, S., Mandler, D., & Long, Y. Simple sol–gel process and one-step annealing of vanadium dioxide thin films: synthesis and thermochromic properties. *Thin Solid Films*, 2013, 534, 594-598.

[65] Seyfouri, M. M., & Binions, R. Sol-gel approaches to thermochromic vanadium dioxide coating for smart glazing application. *Solar Energy Materials and Solar Cells*, 2017, 159, 52-65.

[66] Eslamian, M. Inorganic and organic solution-processed thin film devices. *Nano-Micro Letters*, 2017, 9(1), 3.

[67] Gao, Y., Luo, H., Zhang, Z., Kang, L., Chen, Z., Du, J., ... & Cao, C. Nanoceramic VO2 thermochromic smart glass: A review on progress in solution processing. *Nano Energy*, 2012, 1(2), 221-246.

[68] Liang, X., Chen, M., Guo, S., Zhang, L., Li, F., & Yang, H. Dual-band modulation of visible and near-infrared light transmittance in an all-solution-processed hybrid micro–nano composite film. *ACS Applied Materials & Interfaces*, 2017, 9(46), 40810-40819.

[69] Kagami, Y., Gong, J. P., & Osada, Y. Shape memory behaviors of crosslinked copolymers containing stearyl acrylate. *Macromolecular Rapid Communications*, 1996, 17(8), 539-543.

[70] Ren, Z., Hu, W., Liu, C., Li, S., Niu, X., & Pei, Q. Phase-changing bistable electroactive polymer exhibiting sharp rigid-to-rubbery transition. *Macromolecules*, 2016, 49(1), 134-140.

[71] Li, X. H., Liu, C., Feng, S. P., & Fang, N. X. Broadband light management with thermochromic hydrogel microparticles for smart windows. *Joule*, 2019, 3(1), 290-302.

[72] Zhu, J., Huang, A., Ma, H., Ma, Y., Tong, K., Ji, S., ... & Jin, P. Composite film of vanadium dioxide nanoparticles and ionic liquid–nickel–chlorine complexes with excellent visible thermochromic performance. *ACS Applied Materials & Interfaces*, 2016, 8(43), 29742-29748.

[73] Hu, L., Tao, H., Chen, G., Pan, R., Wan, M., Xiong, D., & Zhao, X. Porous W-doped VO 2 films with simultaneously enhanced visible transparency and thermochromic properties. *Journal of Sol-Gel Science and Technology*, 2016, 77(1), 85-93.

[74] Chiang, F. B. Temperature-responsive hydroxypropylcellulose based thermochromic material and its smart window application. *RSC Advances*, 2016, 6(66), 61449-61453.

[75] Wang, Y., Zhao, F., Wang, J., Li, L., Zhang, K., Shi, Y., ... & Guo, X. Tungsten-doped VO2/starch derivative hybrid nanothermochromic hydrogel for smart window. *Nanomaterials*, 2019, 9(7), 970.

[76] Gupta, R., Rao, K. D. M., Kiruthika, S., & Kulkarni, G. U. Visibly transparent heaters. *ACS Applied Materials & Interfaces*, 2016, 8(20), 12559-12575.

[77] Du Ahn, B., Oh, S. H., Hong, D. U., Shin, D. H., Moujoud, A., & Kim, H. J. Transparent Ga-doped zinc oxide-based window heaters fabricated by pulsed laser deposition. *Journal of Crystal Growth*, 2008, 310(14), 3303-3307.

[78] Jang, H. S., Jeon, S. K., & Nahm, S. H. The manufacture of a transparent film heater by spinning multi-walled carbon nanotubes. *Carbon*, 2011, 49(1), 111-116.

[79] Kiruthika, S., & Kulkarni, G. U. Energy efficient hydrogel based smart windows with low cost transparent conducting electrodes. S*olar Energy Materials and Solar Cells*, 2017, 163, 231-236.

[80] Xie, Z. Silver Nanowire-based Heater: It's Fabrication and Applications in Self-folding Structure and Wearables, 2019.

[81] Bobinger, M., Angeli, D., Colasanti, S., La Torraca, P., Larcher, L., & Lugli, P. Infrared, transient thermal, and electrical properties of silver nanowire thin films for transparent heaters and energy-efficient coatings. *Physica Status Solidi (a)*, 2017, 214(1), 1600466.